RIGA TECHNICAL UNIVERSITY

Ramona Zukule

INVESTIGATION OF ELECTRODES AND ELECTROLYTES FOR OBTAINING AMPHOTERIC DECOUPLED Zn-MnO_2 RECHARGEABLE BATTERIES

Summary of the Doctoral Thesis

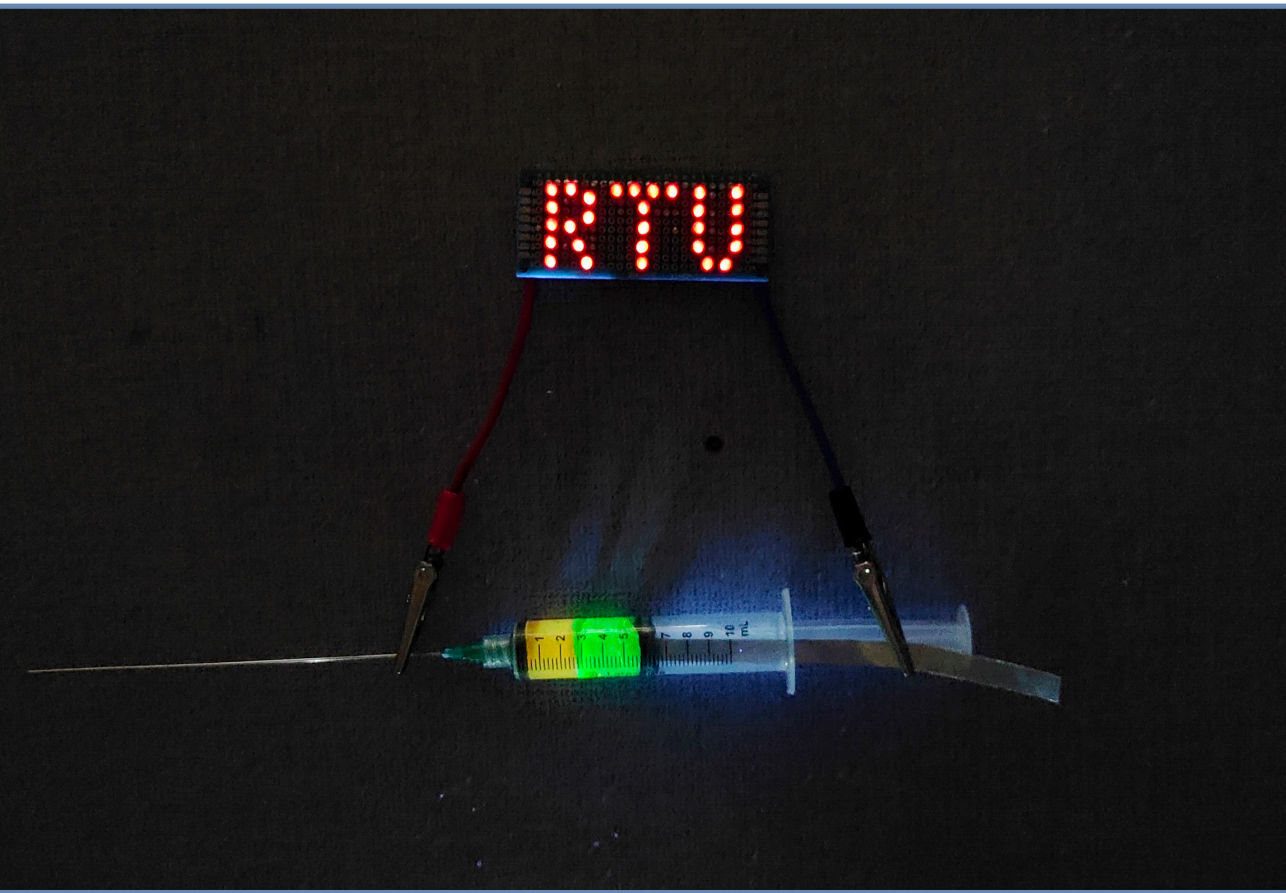

RTU Press
Riga 2025

RIGA TECHNICAL UNIVERSITY
Faculty of Natural Sciences and Technology
Institute of Physics and Materials Science

Ramona Zukule
Doctoral Student of the Study Programme "Chemistry, Materials Science and Engineering"

INVESTIGATION OF ELECTRODES AND ELECTROLYTES FOR OBTAINING AMPHOTERIC DECOUPLED Zn-MnO_2 RECHARGEABLE BATTERIES

Summary of the Doctoral Thesis

Scientific supervisor
Senior Researcher Dr. chem.
REINIS DRUNKA
Senior Researcher Dr. chem.
GUNĀRS BAJĀRS

RTU Press
Riga 2025

Zukule, R. Investigation of Electrodes and Electrolytes for Obtaining Amphoteric Decoupled Zn-MnO_2 Rechargeable Batteries. Summary of the Doctoral Thesis. – Riga: RTU Press, 2025. – 49 p.

Published in accordance with the decision of the Promotion Council "RTU P-02" of September 4, 2025, Minutes No. 04030-9.2/5.

The Doctoral Thesis was developed within the framework of the FLPP project "Investigation of electrodes and electrolytes for obtaining amphoteric decoupled rechargeable batteries" No. lzp-2021/1–0142.

This research was supported

1) by the European Social Fund within the Project No. 8.2.2.0/20/I/008 "Strengthening of PhD students and academic personnel of Riga Technical University and BA School of Business and Finance in the strategic fields of specialization" of the Specific Objective 8.2.2 "To Strengthen Academic Staff of Higher Education Institutions in Strategic Specialization Areas" of the Operational Programme "Growth and Employment";

2) by Riga Technical University's Doctoral Grant programme.

Cover picture by Ramona Zukule.

https://doi.org/10.7250/9789934372353
ISBN 978-9934-37-235-3 (pdf)

ACKNOWLEDGEMENTS

I express my deepest gratitude to all those who have supported and guided me throughout the entire doctoral journey.

First, I would like to extend my heartfelt thanks to my main supervisors, Dr. chem. Gunārs Bajārs and Dr. chem. Reinis Drunka, for their outstanding professional guidance and invaluable feedback. Their in-depth suggestions and constructive criticism significantly contributed to the creation of this Thesis.

I would also like to express sincere gratitude to Dr. phys. Pāvels Onufrijevs, who laid the foundation for both my academic and professional development. His competence, encouragement, and understanding attitude have served as a continuous source of inspiration.

I also appreciate the excellent collaboration with my research group colleagues – PhD Anzelms Zukuls and Ņikita Griščenko – for their support, cooperation, and the enriching discussions during the project development process. Together with my colleagues Mairis Iesalnieks, Linda Laima Alsiņa, and Mārtiņš Vanags, we have participated in many stimulating conversations that not only broadened our horizons but also helped us reach new peaks in our research.

I am equally grateful to the colleagues from the Institute of Physics and Materials Science, as well as to Dr. chem. Nelli Batenko and PhD Anastasija Gaile for their assistance and encouragement, which made my research experience both productive and truly exciting.

Finally, I would like to express my heartfelt gratitude to my life partner and family – whose unwavering love and boundless support were a true pillar throughout this journey. Their faith in me and emotional support were crucial in helping me maintain focus and motivation, even during the most challenging moments.

DOCTORAL THESIS PROPOSED TO RIGA TECHNICAL UNIVERSITY FOR PROMOTION TO THE SCIENTIFIC DEGREE OF DOCTOR OF SCIENCE

To be granted the scientific degree of Doctor of Science (PhD), the present Doctoral Thesis has been submitted for defence at the open meeting of RTU Promotion Council "RTU P-02" on December 10, 2025, in an open meeting online on the Zoom platform: https://rtucloud1.zoom.us/j/96283313764; ID: 962 8331 3764.

OFFICIAL REVIEWERS

Professor Dr. chem. Donāts Erts
University of Latvia, Latvia

Professor PhD Agris Bērziņš
University of Latvia, Latvia

Associate Professor PhD Alar Jänes
University of Tartu, Estonia

DECLARATION OF ACADEMIC INTEGRITY

I hereby declare that the Doctoral Thesis submitted for review to Riga Technical University for promotion to the scientific degree of Doctor of Science (PhD) is my own. I confirm that this Doctoral Thesis has not been submitted to any other university for promotion to a scientific degree.

Ramona Zukule ……. (signature)
Date: ……

The Doctoral Thesis has been prepared as a collection of thematically related scientific publications complemented by summaries in both Latvian and English. The Thesis unites four original research articles and one review article published in Scopus-indexed journals. The scientific publications have been written in English, with a total volume of 57 pages, not including supplementary data.

CONTENTS

ABBREVIATIONS

OCV	open circuit voltage
CB	carbon black
CV	cyclic voltammetry
EIS	electrochemical impedance spectroscopy
GCD	galvanostatic charge-discharge
HER	hydrogen evolution reaction
NMP	N-methyl-2-pyrrolidone
OER	oxygen evolution reaction
SEM	scanning electron microscope
XPS	X-ray photoelectron spectroscopy
XRD	X-ray diffraction

GENERAL OVERVIEW OF THE THESIS

Introduction

Global demand for efficient and sustainable energy storage solutions continues to rise alongside the increasing use of renewable energy sources and the electrification of various sectors [1]–[5]. Renewable energy sources are characterized by irregular energy production – for example, solar energy can only be harnessed during daylight hours [6]–[8]. Therefore, batteries play a crucial role in mitigating the intermittency of renewables by ensuring reliable energy storage and a stable electricity supply on demand [9]–[12]. Currently, one of the most widespread and successful energy storage technologies is rechargeable lithium-ion batteries [13]–[17]. They offer high energy (up to 500 Wh/g) and power (up to 300 W/kg) densities, a large theoretical capacity (890 mA h/g), high operating voltage (> 3.7 V), and excellent charge-discharge stability (over 10,000 cycles) with low self-discharge [18]–[24]. However, key drawbacks of rechargeable lithium-ion batteries include safety concerns due to overheating and potential self-ignition [25]–[29], as well as limited lithium resources [30]–[33]. These issues have prompted the search for alternatives by developing new or improving existing battery technologies.

Among existing battery technologies, aqueous electrolyte Zn-MnO_2 batteries have attracted considerable attention, as they already dominate the non-rechargeable battery market [34], [35]. They offer lower costs, higher safety, and are more environmentally friendly compared to chargeable lithium-ion batteries [36]–[38]. However, to meet future needs, it is necessary to develop their potential application as rechargeable batteries, which presents several challenges, such as electrolyte stability, electrode degradation, and performance limitations [19], [39]–[43].

One of the problems typical for rechargeable Zn-MnO_2 batteries is their low operating voltage and poor cyclability, stemming from the instability of the MnO_2 cathode and unwanted side reactions, such as MnO_2 disproportionation and dissolution, phase transitions to electrochemically inactive forms, oxygen evolution reaction (OER), and the formation of electrochemically inactive compounds with Zn^{2+} ions [44], [45]. To optimize performance, various electrolyte compositions have been studied, including alkaline [19], [38], [46], [47], neutral [48]–[51], and acidic [52], [53] electrolytes. However, each approach undesirably affects cycle life, efficiency, and reaction kinetics. Further adaptation and exploration of electrolytes. i.e., creating pH gradient electrolytes and dual-electrolyte systems, offer significant improvements in electrochemical stability and operating voltage for Zn-MnO_2 systems. By carefully tailoring the electrolyte environment around the anode and cathode, it is possible to extend the electrochemical water decomposition window while mitigating side reactions [54]–[59].

In addition to electrolyte optimization, attention must be paid to the structural stability of the MnO_2 cathode. MnO_2 exists in several polymorphs, each with distinct electrochemical properties depending on its crystal structure. For the sequence $\alpha > \delta > \beta$, the theoretical capacity decreases, meaning the different phases exhibit varying cyclability and ion diffusion properties [60]–[62]. In alkaline electrolytes, the MnO_2 cathode may form electrochemically inactive phases such as $Mn(OH)_2$, Mn_2O_3, and Mn_3O_4 [19], while in acidic environments, it may

dissolve or transition into another polymorph due to side reactions [40], [63], leading to capacity loss. Introducing heteroatoms into the electrode structure is a potential solution to improve electrochemical properties [64]. Studies have explored the effects of heteroatoms on MnO_2 in alkaline and neutral electrolytes. For example, doping with Co [65]–[67] and Mo [68], [69] promotes defect formation in the MnO_2 crystal lattice, stabilizing certain polymorphs. Meanwhile, Bi doping [34], [70]–[73] narrows the MnO_2 bandgap and facilitates electrochemical dissolution–deposition processes

Another key limitation of aqueous Zn-ion batteries is the instability of the metallic Zn anode, which leads to dendrite formation, hydrogen evolution reaction (HER), and surface passivation [41]–[43]. To prevent these side reactions, various surface modification methods have been explored to improve the electrochemical properties of Zn anodes. The main approaches include surface coating and electrolyte modification to control the Zn deposition–dissolution reactions. Coating types include $CaCO_3$ [74], ZnO [75]–[77], ZrO_2 [78]–[80], TiO_2 [81]–[83], and various polymer coatings [84]–[87].

Further development of this research, which includes electrolyte development, cathode stabilization, Zn surface modification, and integration into batteries, is an important step towards the commercialization of rechargeable aqueous electrolyte Zn-MnO_2 batteries. Therefore, this Doctoral Thesis focuses on the main limitations at the electrolyte, cathode, and anode levels with the aim of advancing rechargeable batteries with higher energy density, better cyclability, and improved safety.

Aims and objectives

This Doctoral Thesis aims to develop a concept of increasing the voltage of aqueous Zn-MnO_2 batteries above 2 V and to investigate the required modifications to the electrolyte, cathode, and anode to realize this concept.

To achieve this aim, the following objectives were set:

1. Develop a strategy for increasing the operating voltage of water-based electrolyte rechargeable batteries above 2 V, bypassing the water decomposition voltage limitations.
2. To synthesize MnO_2 powders doped with Bi and Mo ions. To evaluate the properties of the obtained materials using non-destructive analytical methods and prepare thin coatings on carbon paper. To conduct electrochemical measurements of the prepared coatings in an acidic electrolyte solution.
3. To modify Zn plates using pulsed laser irradiation at different energy fluencies. To characterize the prepared samples using non-destructive analysis and perform electrochemical measurements in an alkaline electrolyte solution.
4. To create a pH gradient electrolyte using Pluronic F-127 hydrogel. To assemble a Zn-MnO_2 battery using the pH-gradient electrolyte, conduct electrochemical measurements, and determine whether the operating voltage window of the aqueous electrolyte can be extended beyond 2 V.

Thesis statements to be defended

1. A pH gradient electrolyte system, where there is an alkaline environment at the anode and an acidic environment at the cathode, increases the electrochemical window of water.
2. Doping the MnO_2 cathode with Bi^{3+} and Mo^{6+} ions improves electrochemical performance in acidic electrolyte.
3. The stability of the Zn anode in an alkaline electrolyte is improved by structuring the anode surface with a pulsed laser.
4. A rechargeable amphoteric aqueous electrolyte Zn-MnO_2 battery can be created using Pluronic F-127 micelle-type hydrogel.
5. An aqueous electrolyte Zn-MnO_2 battery with a voltage above 2 V can be obtained by using two different pH electrolytes, or amphoteric systems.

Scientific novelty

In the Doctoral Thesis, an innovative approach to the design of an aqueous Zn-MnO_2 rechargeable battery has been developed and implemented, thus overcoming fundamental limitations at the electrode and electrolyte levels. The study combines strategies in electrode material modification, electrolyte engineering, and battery design improvement to expand the operating voltage range of the battery and improve electrochemical performance. Research has been conducted to improve the stability and electrochemical performance of materials in different pH electrolyte environments, and a new battery concept has been developed based on separated cathode and anode electrolyte spaces. The results of the study reflect the relationships between the structure and properties of water-based electrolyte battery components, which can be used in the development of alternative energy storage systems.

Practical significance

1. Development of aqueous electrolyte Zn-MnO_2 rechargeable batteries with increased operating voltage to promote the development of safer and more efficient alternative energy storage systems.
2. Development of a dual electrolyte system concept that reduces parasitic reactions on the electrodes, thereby improving electrochemical stability, as an alternative to traditional battery designs.
3. Development of scalable methods (doping of semiconductors with heteroatoms via the hydrothermal method and structuring of metal surfaces with a pulsed laser) for modifying electrodes that increase specific capacity.
4. Construction of rechargeable batteries using elements commonly found in the Earth's crust as electrode materials, creating an alternative battery technology that does not depend on critical raw materials.

Structure and volume of the Thesis

The Doctoral Thesis is presented as a thematically unified collection of scientific publications focused on the development of an amphoteric aqueous Zn-MnO_2 battery and the individual improvement of its electrolyte and electrodes. The Thesis includes four original research articles and one review article published in Scopus-indexed journals.

Publications and approbation of the Thesis

The main results of the Thesis are published in four scientific research articles. One review article was also prepared during the development of the Thesis. The research results have been presented at 17 scientific conferences.

Scientific publications

1. **R. Durena**, N. Griscenko, L. Orlova, M. Bertins, A. Viksna, M. Iesalnieks, A. Zukuls. Synthesis, structure, and electrochemical performance of Bi-induced stabilization of MnO_2 cathodes for use in highly acidic aqueous electrolytes (pH < 2). *Journal of Alloys and Compounds*, 1010, **2025**, 177904. https://doi.org/10.1016/j.jallcom.2024.177904 (*IF 5.8, CiteScore 11.1*)
2. **R. Dūrena**, L. Fedorenko, Ņ. Griščenko, M. Vanags, L. Orlova, P. Onufrijevs, S. Stanionyte, T. Malinauskas, A. Zukuls. Irradiating the Path to High-Efficiency Zn-Ion Batteries: An Electrochemical Analysis of Laser-Modified Anodes. *Global Challenges*, 8 (10), **2024**, 2400105. https://doi.org/10.1002/gch2.202400105 (*IF 4.4, CiteScore 8.7*)
3. Ņ. Griščenko, **R. Dūrena**, M. Iesalnieks, M. Bērtiņš, A. Vīksna, A. Zukuls. Improvement of manganese dioxide cathode by molybdenum doping in highly acidic electrolyte. *Journal of Energy Storage*, 76, **2024**, 109847. https://doi.org/10.1016/j.est.2023.109847 (*IF 8.9, CiteScore 11.8*)
4. **R. Durena**, A. Zukuls. A Short Review: Comparison of Zinc–Manganese Dioxide Batteries with Different pH Aqueous Electrolytes. *Batteries*, **2023**, 9(6), 311. https://doi.org/10.3390/batteries9060311 (*IF 5.3*)
5. **R. Durena**, A. Zukuls, M. Vanags, A. Šutka. How to increase the potential of aqueous Zn-MnO_2 batteries: The effect of pH gradient electrolyte. *Electrochimica Acta*, **2022**, 434, 141275. https://doi.org/10.1016/j.electacta.2022.141275 (*IF 5.5, CiteScore 11.3*)

Most significant conference participation

1. **R. Dūrena**, Ņ. Griščenko, A. Zukuls. High-Potential 2 V Rechargeable Zinc-Manganese Dioxide Batteries Enabled by Polymer Hydrogels. *2024 MRS Fall Meeting*. Boston, USA. 1–6 December **2024**. EN08.08.25
2. **R. Dūrena**, Ņ. Griščenko, A. Zukuls. Extending the Electrochemical Window of Aqueous Zn-MnO_2 Batteries through pH Gradient Dual-Electrolyte. *Battery 2030+'s 4th Annual Conference & Young Scientists gathering*. Grenoble, France. 27–29 May **2024**. P37

3. **R. Dūrena**, Ņ. Griščenko, A. Zukuls. Enhanced capacity retention of MnO_2 cathode enabled by Bi doping. *8th Baltic Electrochemistry Conference: Finding New Inspiration 2*. Tartu, Estonia. 14–17 April **2024**. P24
4. **R. Dūrena**, A. Zukuls, M. Vanags. Amphoteric Zinc-Manganese Dioxide Aqueous Battery Exceeding 2V Potential. *16th International Conference on Materials Chemistry*. Dublin, Ireland. 3–6 June **2023**. P256
5. **R. Dūrena**, A. Zukuls, M. Vanags. 2.4 V Open-Circuit Potential Aqueous Zn-MnO_2 Rechargeable Battery with pH gradient hydrogel electrolyte. *European Materials Research Society Spring Meeting*. Strasbourg, France, 29.05–02.06, **2023**. D_P01-33.

LITERATURE REVIEW AND RESULTS

Literature review and results of the Doctoral Thesis are presented in four main chapters, which combine one review article and four original publications:

1. Literature review on the performance of an aqueous electrolyte Zn-MnO_2 battery depending on the pH of the electrolyte medium, as well as an evaluation and explanation of the dual battery concept, summarizing the review article (Appendix 1).
2. Results of the research on improving the operation and performance of MnO_2 cathode in a highly acidic electrolyte by incorporating Bi and Mo ions into the MnO_2 structure, summarized in original Publication 1 (Appendix 2) and original Publication 2 (Appendix 3).
3. Results of the research on improving the operation and performance of Zn anode in alkaline electrolyte using surface structuring with a high-power pulsed laser, summarized in original Publication 3 (Appendix 4).
4. Results of the research on the development and electrochemical parameters of a dual aqueous electrolyte Zn-MnO_2 rechargeable battery, summarized in original Publication 4 (Appendix 5).

1. Literature review on the performance of an aqueous electrolyte Zn-MnO_2 battery depending on the pH of the electrolyte medium

The origins of aqueous electrolyte Zn-MnO_2 batteries date back to 1866, when French scientist Georges Leclanché manufactured and patented the first Zn-MnO_2 non-rechargeable battery, called the Leclanché cell [7]. These batteries were further developed in the 1950s by Canadian engineer Lewis Urry, who patented the alkaline Zn-MnO_2 battery in 1960 [88]–[91]. These batteries are still being improved, trying to extend their effective lifespan and replace hazardous elements such as mercury. Thus, aqueous alkaline Zn-MnO_2 batteries are the longest-standing and most widely used non-rechargeable battery technology, still dominating the global market [92]. This could be due to the fact that aqueous electrolyte Zn-MnO_2 batteries do not pose major safety risks, Zn metal has low toxicity (LD50 = 630 mg/kg – in rats) [93], Zn^{2+}/Zn two-electron reaction has a relatively high theoretical capacity of 820 mAh/g [36], [37], as well as the theoretical capacity of MnO_2/Mn^{2+} two-electron reaction is 617 mAh/g [38], [94], [.95]. Moreover, both zinc and manganese are common elements in the Earth's crust [36], [37].

1.1. Alkaline electrolyte Zn-MnO_2 batteries

An aqueous alkaline Zn-MnO_2 battery consists of a Zn metal anode, a MnO_2 cathode, and a concentrated KOH aqueous solution (> 30 %) electrolyte. Carbon black (CB) particles are usually added to the cathode to ensure its conductivity, as MnO_2 itself is non-conductive. The schematic of this non-rechargeable battery is shown in Fig. 1.1, where the Zn anode undergoes electrochemical Reaction (1) with a standard potential of –1.199 V, while the cathode active component MnO_2 undergoes Reactions (2) and (3) with a standard potential of +0.250 V. Thus,

overall Reaction (4) occurs in the alkaline battery, resulting in an OCV of 1.45 V for the battery [6], [94], [96], [97].

Anode: $Zn + 4OH^- \rightarrow Zn(OH)_4^{2-} + 2e^-$ $E^0 = -1.20\ V$ (1)

Cathode: $MnO_2 + H_2O + e^- \rightarrow MnOOH + OH^-$ $(1^{st}\ e^-)$ $E^0 = +0.25\ V$ (2)

$MnOOH + H_2O + e^- \rightarrow Mn(OH)_2 + OH^-$ $(2^{nd}\ e^-)$ (3)

Overall reaction:

$Zn + MnO_2 + 2H_2O + 2OH^- \rightarrow Zn(OH)_4^{2-} + Mn(OH)_2$ $E = 1.45\ V$ (4)

Alkaline Zn-MnO_2 batteries are a long-established technology and are still being researched. Although these batteries are widespread as non-rechargeable batteries, they are still not widespread as rechargeable batteries. This is mainly due to the formation of electrochemically inactive manganese oxides Mn_3O_4 and $ZnMn_2O_4$. These compounds are formed during the deep discharge process [88], [98]. Thus, during the first few discharge-charge cycles, electrochemically inactive compounds cover the particles of the active MnO_2 compound of the cathode, stopping further reaction, which rapidly reduces the battery capacity. The scientific literature describes various ways to reduce or eliminate this undesirable effect in alkaline electrolytes, for example, doping the MnO_2 cathode with Bi or Cu ions [94], [99], as well as modifying the electrolyte by adding extra ions [100]–[102], such as Li^+ [98].

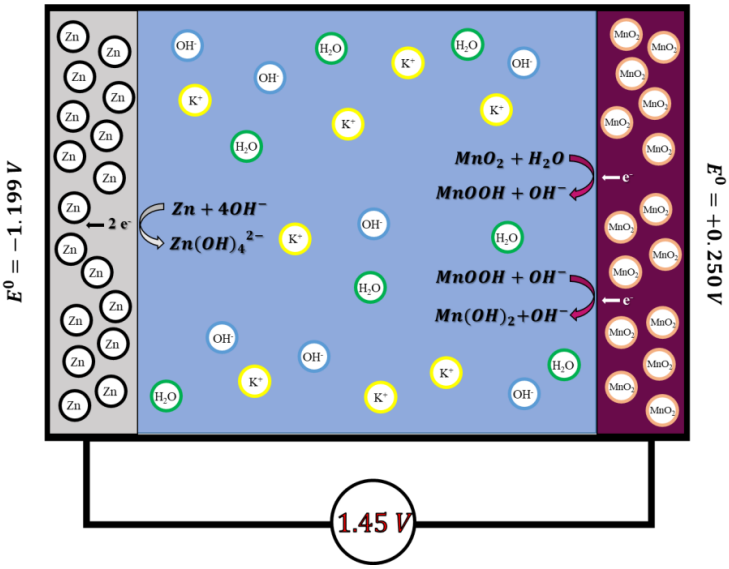

Fig. 1.1. Schematic operating mechanism of Zn-MnO_2 batteries with an alkaline aqueous electrolyte.

1.2. Neutral and acidic electrolyte Zn-MnO_2 batteries

The modification of the electrolyte in Zn-MnO_2 batteries has been further advanced by reducing the pH of the electrolyte from alkaline to neutral and even acidic, thereby altering the overall reactions occurring in the battery, as illustrated in the schematic representation of the Zn-MnO_2 battery with an acidic aqueous electrolyte (Fig. 1.2). In these systems, the alkaline electrolyte composed of KOH, NaOH, and LiOH [97], [98], [103]–[105] has been replaced with solutions of $ZnSO_4$, $MnSO_4$, K_2SO_4, Na_2SO_4 [106]–[111] and/or a diluted acid electrolyte [52], [53]. As shown in the Pourbaix diagram of manganese compounds (Fig. 1.3 a), which depicts the changes in the standard potential of the element in an aqueous electrolyte depending on the pH, at higher pH values, the electrochemical reaction of MnO_2 occurs at a standard potential of 0.250 V, with the possibility of forming the electrochemically inactive Mn_2O_3 phase. However, when the electrolyte pH is lowered to an acidic level, the oxygen atom in the MnO_2 cathode can bind with H^+ ions from the electrolyte, forming water molecules. Consequently, Mn^{4+} ions can be reduced to Mn^{2+} ions, which dissolve into the electrolyte solution without forming the electrochemically inactive Mn_2O_3 phase. Moreover, this MnO_2 reaction in an acidic medium occurs at a standard potential above 1.2 V. However, this reduction in electrolyte pH increases the electrochemical reaction potential of the Zn anode. As seen in the Pourbaix diagram of zinc compounds (Fig. 1.3 b), the standard potential of the reaction increases from –1.199 V in an alkaline medium to –0.762 V in an acidic medium.

Despite the increase in the standard potential of the Zn anode, the overall battery design results in a higher operating voltage of up to 2 V, according to Reactions (5)–(7) [112]:

Anode: $Zn \rightarrow Zn^{2+} + 2e^-$ $E^0 = -0.76\,V$ (5)

Cathode: $MnO_2 + 4H^+ + 2e^- \rightarrow Mn^{2+} + 2H_2O$ $E^0 = +1.22\,V$ (6)

Overall reaction:

$Zn + MnO_2 + 4H^+ \rightarrow Zn^{2+} + Mn^{2+} + 2H_2O$ $E = 1.98\,V$ (7)

However, in an acidic medium, a parasitic reaction occurs – Zn anode corrosion. During this process, the Zn anode dissociates into Zn^{2+} ions in the electrolyte, releasing H_2 gas. This parasitic reaction not only reduces the capacity of the battery but can also lead to the rupture of the battery cell [113]. The occurrence of the parasitic reaction at the anode can be mitigated by coating the Zn anode with fumed silica and polyethylene glycol (with a molecular weight of 300 g/mol) [114]. To prevent potential MnO_2 dissolution, 0.1 M $MnSO_4$ is added to the electrolyte [107]–[110]. However, even in this type of battery, the formation of the $ZnMn_2O_4$ phase has been observed, which is chemically inactive and leads to capacity fading by increasing reaction irreversibility [115]. This suggests that both alkaline and neutral-acidic aqueous electrolyte Zn-MnO_2 batteries face similar challenges.

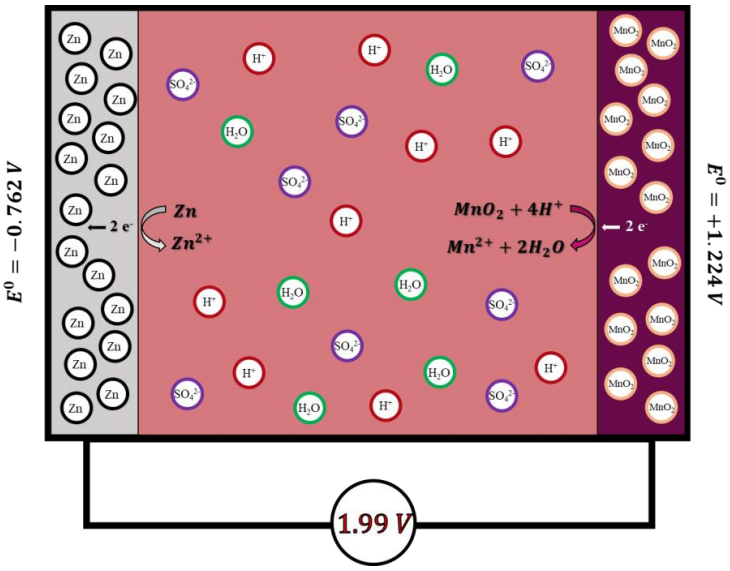

Fig. 1.2. Schematic operating mechanism of Zn-MnO_2 batteries with an acidic aqueous electrolyte.

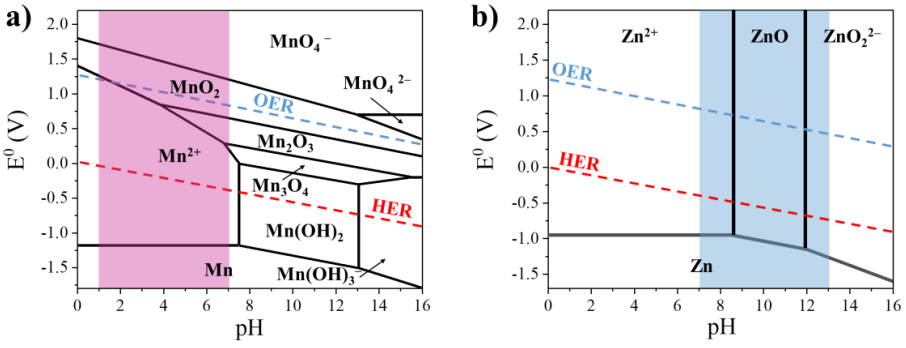

Fig. 1.3. Pourbaix diagrams with marked water decomposition potentials: a) for manganese compounds, and b) for zinc compounds [116].

1.3. Dual/amphoteric electrolyte Zn-MnO_2 batteries

To combine the beneficial properties of both alkaline and acidic aqueous electrolytes, a new type of cell has been developed, enabling an increase in the water decomposition voltage above 2 V. The structure of this cell consists of two electrolytes with different pH mediums, allowing the Zn anode to operate in an alkaline electrolyte while the MnO_2 cathode functions in an acidic electrolyte. This unique battery design, whose operating principle is illustrated in Fig. 1.4,

enhances the open-circuit voltage (OCV) of the cell up to 2.45 V, according to Reactions (8)–(10) [54], [113], [114].

Anode: $Zn + 4(OH)^- \rightarrow Zn(OH)_4^{2-} + 2e^-$ $E^0 = -1.20\ V$ (8)

Cathode: $MnO_2 + 4H^+ + 2e^- \rightarrow Mn^{2+} + 2H_2O$ $E^0 = +1.22\ V$ (9)

Overall reaction:

$Zn + 4(OH)^- + MnO_2 + 4H^+ \rightarrow Zn(OH)_4^{2-} + Mn^{2+} + 2H_2O$ $E = 2.42\ V$ (10)

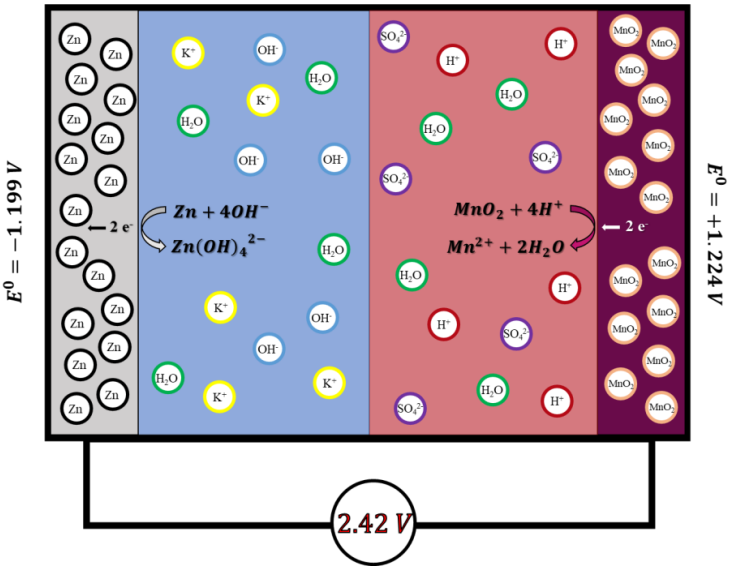

Fig. 1.4. Schematic operating mechanism of Zn-MnO_2 batteries with dual/amphoteric aqueous electrolyte.

The expanded water decomposition voltage window can also be explained using the Pourbaix diagram. As shown in Fig. 1.5, when the battery cell consists of a single electrolyte with a constant pH, the water decomposition voltage is 1.23 V. Consequently, using an aqueous electrolyte battery within a wider voltage window can lead to undesirable OER and HER. However, by employing a dual/amphoteric electrolyte system, it is possible to achieve a stable electrochemical voltage window for the aqueous electrolyte exceeding 2 V. Moreover, considering that, according to the Tafel equation, hydrogen evolution on Zn exhibits a high overpotential [117], [118], while oxygen evolution has a high overpotential [56] and slow reaction kinetics [119], the usable voltage range of the aqueous electrolyte can be extended up to 3 V.

Overall, the concept of a dual-electrolyte system and an expanded water stability voltage window has been described since 2005 [55]–[57]. Later, this dual-electrolyte concept was also applied to various battery systems, including Al-air [120]–[123], Zn-air [121], [124], [125], Mg-air [121], [126], Zn-PbO_2 [127]–[129], Zn-Br_2 [130], and Zn-MnO_2 [54], [58], [131].

However, the operational lifespan and efficiency of all these batteries are limited by neutralization reactions and ion diffusion within the electrolyte.

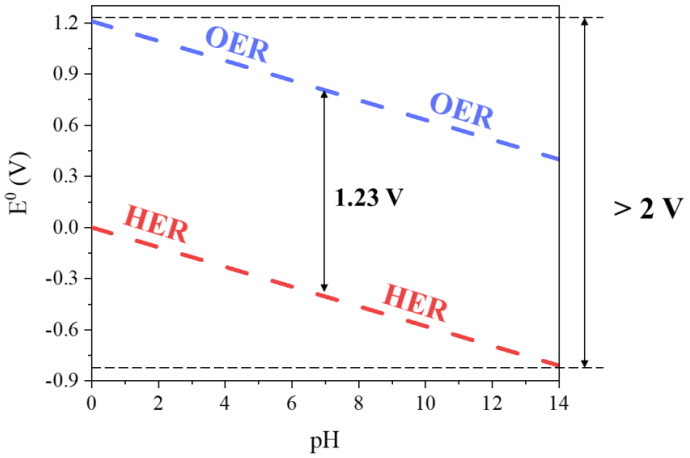

Fig. 1.5. Water Pourbaix diagram [116].

2. Main results about the improvement of MnO_2 cathode performance in acidic electrolyte

This chapter describes the improvement of MnO_2 cathode performance in a highly acidic (pH < 2) aqueous electrolyte by doping MnO_2 with Bi and Mo ions. The effect of the dopant ions is evaluated by investigating the impact of Bi and Mo ion concentration on the structural and electrochemical properties of MnO_2, with concentrations ranging from 0 mol% to 10 mol%. Additionally, the mechanical role of Bi and Mo in stabilizing MnO_2 during the charge-discharge cycles is also examined.

2.1. Methodology

Bi- and Mo-doped MnO_2 powders were synthesized via a hydrothermal method using $KMnO_4$ as the manganese precursor. $BiCl_3$ was used as the bismuth precursor and introduced in concentrations ranging from 0 mol% to 10 mol%, while Na_2MoO_4 was used for Mo-doped samples in concentrations from 0 mol% to 5 mol%. The required salts for each synthesis were dissolved in distilled water, with a fixed amount of CB additionally introduced. The resulting solution was placed in an autoclave and kept in an oven at 120 °C for either 12 h or 24 h. After the hydrothermal synthesis, all obtained powder samples were thoroughly washed with distilled water and dried in an oven at 60 °C for 24 h.

Additionally, a commercially obtained MnO_2 (in the pyrolusite phase or β-MnO_2) sample was studied as a reference for the synthesized samples. To fabricate the cathodes, pyrolusite

and obtained powder samples were mixed with additional CB in a 13 : 5 ratio to improve the conductivity of the cathode. A cathode slurry was then prepared from the powder mixture by adding a polyvinylidene fluoride solution in N-methyl-2-pyrrolidone (NMP) in a 1 : 9 ratio. The resulting slurry was applied onto carbon paper using a doctor blade, followed by NMP evaporation and cutting the electrodes to the required dimensions.

2.2. Results

2.2.1. Bi-doped MnO_2 cathode

According to the XRD results shown in Fig. 2.1 a, the synthesized samples exhibited a two-phase mixture consisting of δ-MnO_2 ($Mn_7O_{13}{\cdot}5\ H_2O$ – birnessite) and α-MnO_2 ($K_{2-x}Mn_8O_{16}$ – hollandite). Additionally, at higher dopant concentrations, the formation of a BiOCl phase was observed. Increasing the Bi ion concentration in the samples resulted in a decrease in the intensity of the δ-MnO_2 phase peak at 24.6º and an increase in the intensity of the α-MnO_2 phase peaks at 29º and 42º. This suggests that the introduction of Bi ions promotes the formation of the α-MnO_2 phase, which exhibits a 2 × 2 tunnel-like crystal structure. In this case, Bi ions occupy the vacant sites in the MnO_2 2 × 2 tunnel structure as a filler. This prevents MnO_2 from adopting the layered δ-MnO_2 structure [70], [72], [132]–[134]. The formation of the tunnel-like α-phase is preferable in this context, as its tunnel structure facilitates ion transport through the crystal lattice, thereby enhancing electrochemical kinetics. In contrast, MnO_2 without dopant ions predominantly exhibited a phase more susceptible to dissolution in acidic environments. Scanning electron microscopy (SEM) images of the samples, shown in Fig. 2.1 b, reveal that the synthesized powders consist of aggregates of smaller and larger needle-like structures, which are characteristic of different MnO_2 polymorphs [135]–[137]. In comparison, the pyrolusite reference sample consists of rounded particle aggregates.

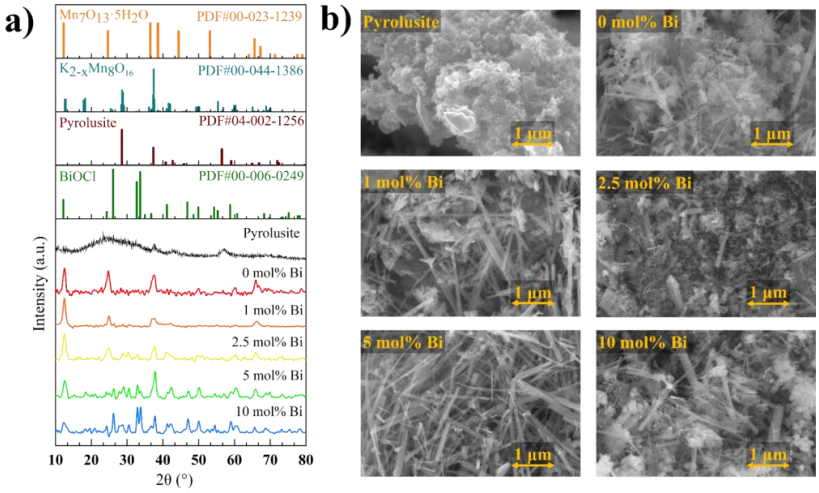

Fig. 2.1. Bi-doped MnO_2 sample and pyrolusite: a) XRD diffractograms, and b) SEM images.

To further characterize the synthesized samples, X-ray photoelectron spectroscopy (XPS) analysis was performed. In the normalized Mn 2p XPS spectra (Fig. 2.2 a), a peak shift towards the Mn^{3+} binding energy is observed, which becomes more pronounced with increasing Bi^{3+} concentration in the sample. Additionally, the differential spectra of the normalized XPS signals (Fig. 2.2 b) show a decrease in the Mn^{4+} signal and an increase in the Mn^{3+} signal as the Bi^{3+} concentration increases. Similar observations regarding the formation of Mn^{3+} and Mn^{4+} oxidation states under comparable synthesis conditions in various metal oxide systems have been reported in the literature [138], [139]. These studies explain the role of heteroatoms introduced into the MnO_2 crystal structure in stabilizing metastable Mn^{3+} ions, which typically undergo disproportionation in oxide crystal lattices [140]. In the normalized O 1s spectra (Fig. 2.2 c), an increase in hydroxyl groups and adsorbed water on the surface is observed with higher Bi^{3+} concentrations in the sample. According to literature data, binding energies in the range of 531–535 eV are closely associated with surface hydroxyl groups, water, or oxygen-containing organic byproducts [141]. Examining the Bi 4f XPS spectra (Fig. 2.2 d), no Bi signal is detected in the 0 mol% Bi sample. However, as the Bi^{3+} concentration increases, the Bi signal becomes more pronounced, confirming that all Bi-containing samples have Bi atoms in the 3+ oxidation state [142], [143].

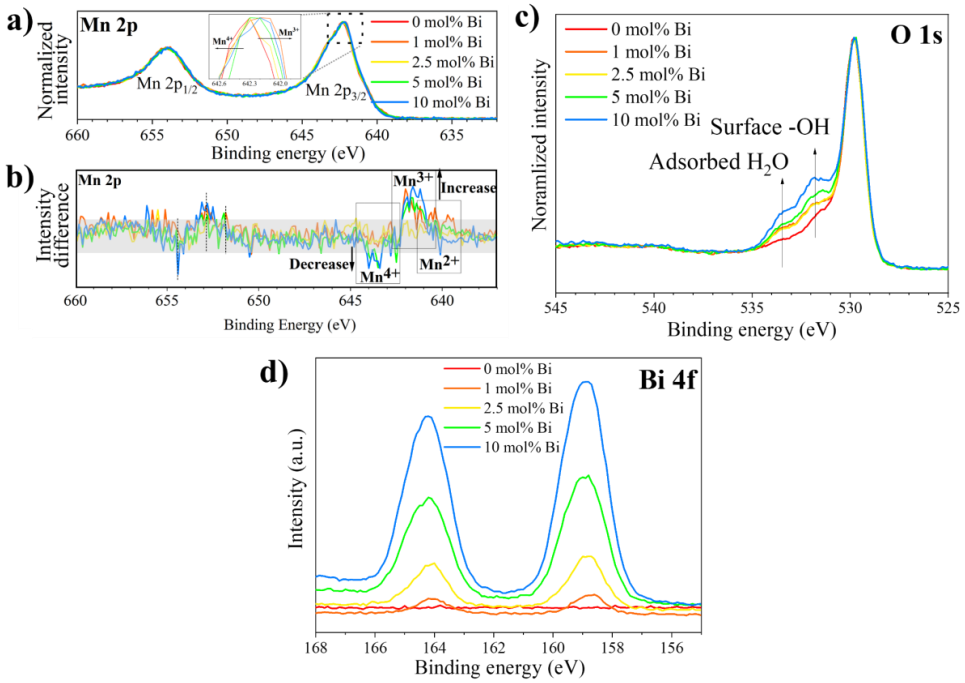

Fig. 2.2. Bi-doped MnO_2 sample and pyrolusite: a) normalized Mn 2p XPs spectra, and b) difference thereof; c) Bi 4f spectra, and d) normalized O 1s spectra.

Cyclic voltammetry (CV) measurements were performed on the prepared cathodes, and the specific capacities of each cathode were calculated based on the obtained data, as shown in Fig. 2.3 a. From these results, at slower scan rates, the cathode with 5 mol% Bi ion content exhibits the highest specific capacity of 130 mAh/g, while the cathode without Bi ions reaches only 120 mAh/g, and the pyrolusite cathode achieves 90 mAh/g.

To evaluate the capacity retention, galvanostatic charge-discharge (GCD) measurements were performed at varying current densities, as shown in Fig. 2.3 b. During the first five cycles, material activation and cathode stabilization take place. The pyrolusite cathode and the cathode without Bi ions require all five cycles to fully stabilize. In contrast, samples containing Bi ions stabilize within 2–3 cycles. In the following 15 cycles, as the current density increases from 0.25 A/g to 1.0 A/g, the pyrolusite cathode exhibits a similar capacity to the cathodes containing 0–5 mol% Bi ions. However, when the current density is reduced back to the initial 0.25 A/g, cathode materials with a higher Bi ion content demonstrate better capacity retention.

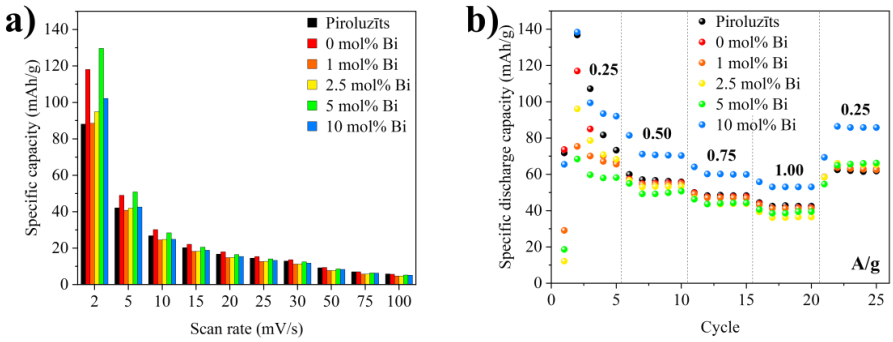

Fig. 2.3. Specific capacities of Bi-doped MnO_2 samples and pyrolusite: a) specific capacities obtained from CV measurements at different scan rates, and b) specific discharge capacities from GCD measurements at different current densities.

The electrochemical impedance spectroscopy (EIS) results for all samples after CV measurements are shown in the EIS diagrams in Fig. 2.4 a, where two compressed semicircles can be observed – one at high frequencies and the other at low frequencies. Additionally, fitted curves are shown based on the equivalent circuit in Fig. 2.4 b. The circuit consists of resistances – R_s, R_1, and R_2 – and constant phase elements – CPE_1 and CPE_2 – parallel to their respective resistances. The values of all these components are listed in Table 2.1. The ohmic resistance of the electrolyte corresponds to component R_s and is approximately 22–23 Ω for all samples. The resistance R_1 and constant phase element CPE_1 represent the charge transfer resistance between the electrode and electrolyte as well as the double-layer capacitance. The fitted values indicate that the hydrothermally synthesized cathode materials exhibit a reduced double-layer capacitance, with the most significant reduction observed for the 10 mol% Bi MnO_2 sample. This observation correlates with the increase in surface hydroxyl groups shown in Fig. 2.2 c. The variation in surface hydroxyl group content influences the wetting properties of the

electrode and affects the interaction between the electrode surface and the electrolyte, thereby impacting the charge transfer resistance. The second set of parallel components – resistance R_2 and constant phase element CPE_2 – corresponds to the overall resistance and capacitance between individual cathode particles, since the cathode consists of a mixture of individual semiconductor MnO_2 and CB particles. According to the fitted values, the synthesized samples exhibit significantly lower resistance between individual particles. Comparing the pyrolusite and 0 mol% Bi samples, the CB added during synthesis reduces the particle-to-particle resistance by more than nine times.

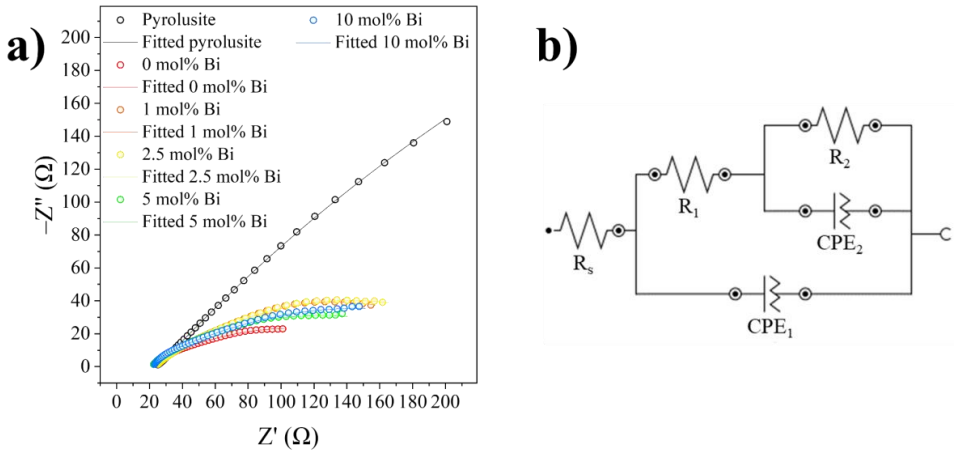

Fig. 2.4. Bi-doped MnO_2 sample and pyrolusite: a) measured EIS diagrams with fitted data according to b) equivalent circuit.

Table 2.1

Equivalent Circuit Parameters of the EIS Fitted Data

Sample	R_s	R_1	CPE_1		R_2	CPE_2		χ^2
			Y^0	N		Y^0	N	
	Ω	Ω	$mS \cdot s^N$		Ω	$mS \cdot s^N$		
Pyrolusite	23.82	5.05	1.13	0.54	1474.8	1.93	0.52	0.00039
0 mol% Bi	21.66	9.49	0.29	0.68	161.94	6.30	0.34	0.00045
1 mol% Bi	23.75	49.03	1.52	0.52	162.74	3.32	0.45	0.00106
2.5 mol% Bi	23.74	39.57	1.38	0.53	195.00	3.54	0.40	0.00148
5 mol% Bi	21.71	6.23	0.16	0.74	204.60	4.68	0.36	0.00208
10 mol% Bi	22.37	8.04	0.13	0.77	242.74	4.80	0.35	0.00210

2.3.2. Mo-doped MnO_2 cathode

Also, XRD diffractograms shown in Fig. 2.5 for the Mo-doped samples reveal the presence of two phases: δ-MnO_2 ($Mn_7O_{13}·5H_2O$ – birnessite) and α-MnO_2 ($K_{2-x}Mn_8O_{16}$ – hollandite). Similar to the Bi-doped samples, an increase in Mo concentration leads to a decrease in the δ-MnO_2 phase and an increase in the α-MnO_2 phase. This indicates that the addition of Mo dopant promotes the formation of the α-MnO_2 phase. Additionally, the synthesis time influences the crystallinity of the samples, as evidenced by more pronounced diffraction peaks in the samples synthesized for 24 hours with Mo concentration up to 2.5 mol%. This suggests the formation of larger crystallites [144], which is also consistent with the SEM images shown in Fig. 2.6 a. In these images, the samples synthesized for longer durations exhibit more defined structures, whereas the 12-hour samples consist of randomly shaped agglomerates.

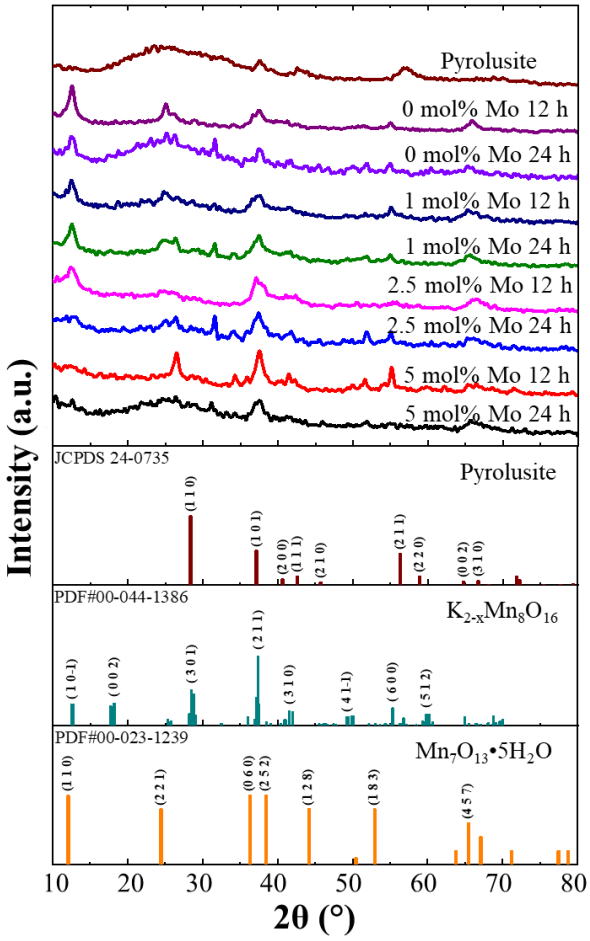

Fig. 2.5. XRD diffractograms of Mo-doped MnO_2 samples and pyrolusite.

XPS analysis was also performed to determine the oxidation states of the elements present, with the spectra shown in Fig. 2.6 b. All samples contain Mn^{4+} ions, and the synthesized samples also exhibit carbon-oxygen bonds due to the addition of CB during the synthesis process. Furthermore, the Mo-doped MnO_2 samples contain Mo^{6+} ions and metastable Mn^{3+} ions, indicating that the addition of Mo ions also stabilizes Mn^{3+} ions [145].

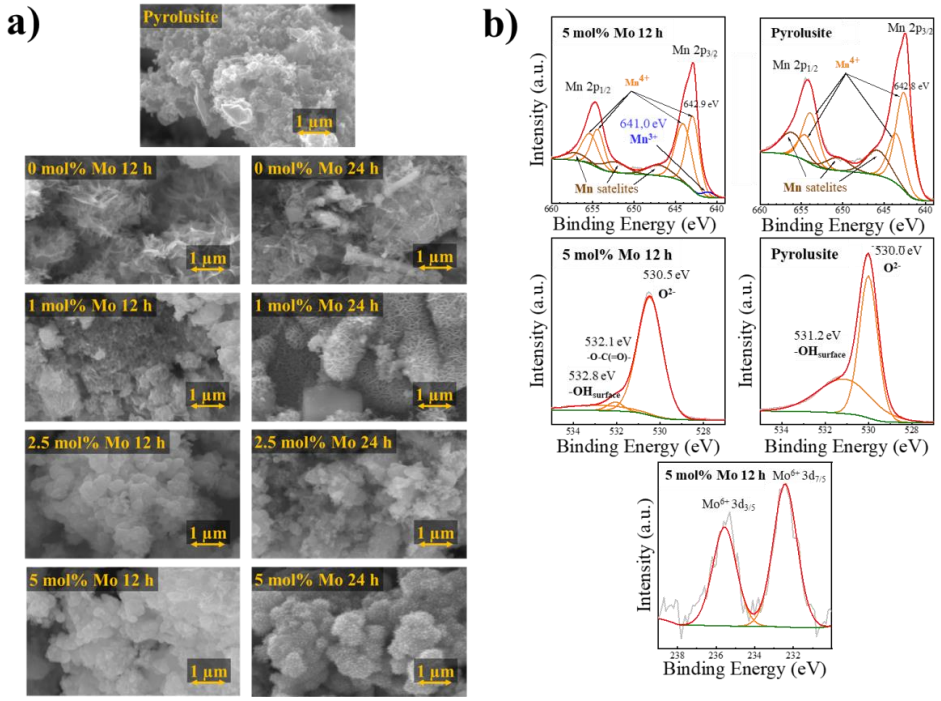

Fig. 2.6. Mo-doped MnO_2 sample and pyrolusite: a) SEM images, and b) Mn 2p, O 1s and Mo 3d spectra.

Further cathodes were prepared from Mo-doped MnO_2 samples, and CV measurements were performed to calculate the specific capacities of each cathode, which are summarized in Fig. 2.7 a. All synthesized samples show a higher specific capacity than the pyrolusite sample, with the specific capacity of the synthesized samples increasing as Mo atoms are added. The general increase in specific capacity between the pyrolusite and synthesized samples may be related to phase differences, as seen in the XRD results (Fig. 2.5), where the synthesized samples contain both δ-MnO_2 and α-MnO_2 phases. The highest specific capacity, 415 mAh/g at 0.002 V/s, was obtained from the 2.5 mol% Mo-doped MnO_2 sample synthesized for 12 hours. However, further tests reveal that the 1 mol% Mo-doped sample, synthesized for 12 hours, retains its specific capacity better as the scan rate increases. Overall, the CV measurements indicate that Mo-doped samples show an increase in specific capacity up to a Mo concentration of 2.5 mol%.

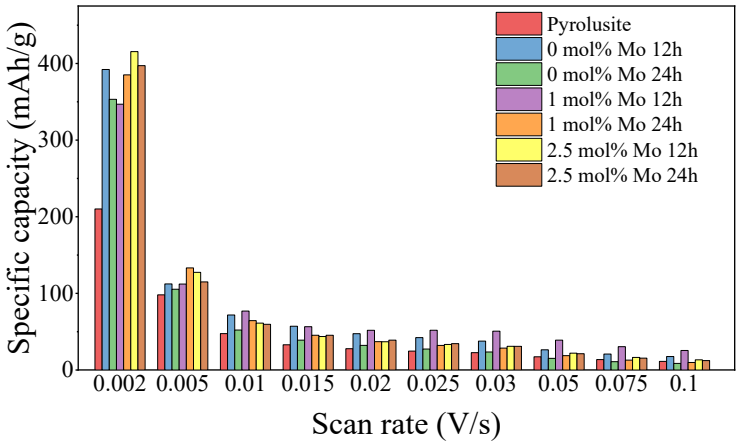

Fig. 2.7. Specific capacities of Mo-doped MnO_2 samples and pyrolusite.

3. Main results about improving the performance of the Zn anode in alkaline electrolyte

This chapter describes the improvement of the electrochemical properties of the zinc anode achieved by irradiating the Zn surface with a pulsed laser. The effect of laser irradiation on the structural and morphological properties of the Zn anode was evaluated. The electrochemical properties of the obtained anode materials, such as surface-specific capacity and charge transfer resistance, were examined. Possible mechanisms for the influence of laser modification on the performance of Zn anodes are discussed.

3.1. Methodology

Zinc plates with 99.95 % purity were modified using a nanosecond pulsed Nd: YAG laser at two wavelengths (266 nm and 1064 nm) in air and deionized water environments. A schematic of the irradiation process is shown in Fig. 3.1. The main laser parameters – energy fluence (ranging from 0.32 J/cm^2 to 2.66 J/cm^2), which varies depending on the irradiation process, and pulse duration (6 ns) – were systematically varied and are summarized in Table 3.1. The resulting Zn anode samples were tested in an electrochemical half-cell with a 1 M KOH electrolyte, a Pt counter electrode, and an Ag/AgCl (3M KCl) reference electrode following surface examination.

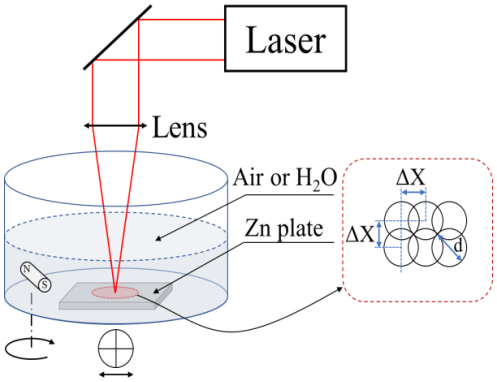

Fig. 3.1. Schematic representation of the laser irradiation process.

Table 3.1

Laser Irradiation Parameters

Sample*	Laser wavelength, nm	Irradiation medium	Energy fluence, J/cm^2
Zn	un-irradiated	–	–
Zn-A-2.66*	266	Air	2.66
Zn-A-0.38	1064	Air	0.38
Zn-A-0.59	1064	Air	0.59
Zn-A-0.64	1064	Air	0.64
Zn-A-0.71	1064	Air	0.71
Zn-W-0.32*	266	Deionized water	0.32
Zn-W-0.53*	266	Deionized water	0.53
Zn-W-0.69	1064	Deionized water	0.69
Zn-W-1.29	1064	Deionized water	1.29
Zn-W-1.42	1064	Deionized water	1.42
Zn-W-1.60	1064	Deionized water	1.60

*A – air medium, W – water medium.

3.2. Results

Irradiation of samples with a pulsed laser caused significant morphological changes on the surface, as seen in SEM micrographs (Fig. 3.2). The untreated zinc sample exhibits a smooth surface with cold rolling marks characteristic of the manufacturing process, while the laser-treated samples display various surface morphologies depending on the irradiation environment. Samples irradiated in air with a 1064 nm laser show intense melting during irradiation, resulting in frozen droplet-like structures on the surface. In contrast, samples

irradiated in water with the same wavelength reveal wrinkled structures with homogeneously distributed droplets underneath. Samples irradiated in air with a 266 nm laser exhibit a moderately melted surface with a more uniform texture, whereas irradiation in water induces ZnO growth and forms a wrinkled melt structure.

XRD (Theta/2theta) diffractograms of untreated Zn plates (Fig. 3.3 a) show a polycrystalline Zn pattern with a dominant (002) basal plane parallel to the surface of the sheet. This is related to deformations caused during rolling in the production process [146]. However, Laser treatment of the samples reduces the intensity of the dominant (002) basal plane in the diffractograms. This is due to the surface melting caused by the laser, revealing the underlying polycrystalline structure where the (101) plane dominates. These changes promote more uniform zinc deposition during electrochemical processes. However, Raman spectra shown in Fig. 3.3 b confirm the formation of hexagonal ZnO on the surfaces of the irradiated samples. Additionally, Raman spectra reveal various ZnO defects: oxygen vacancies (A_1(LO) peak at 574 cm^{-1}), interstitial Zn atoms (broad peak between 250–300 cm^{-1}), and nitrogen-related defects (peak at 275 cm^{-1}) [147], [148].

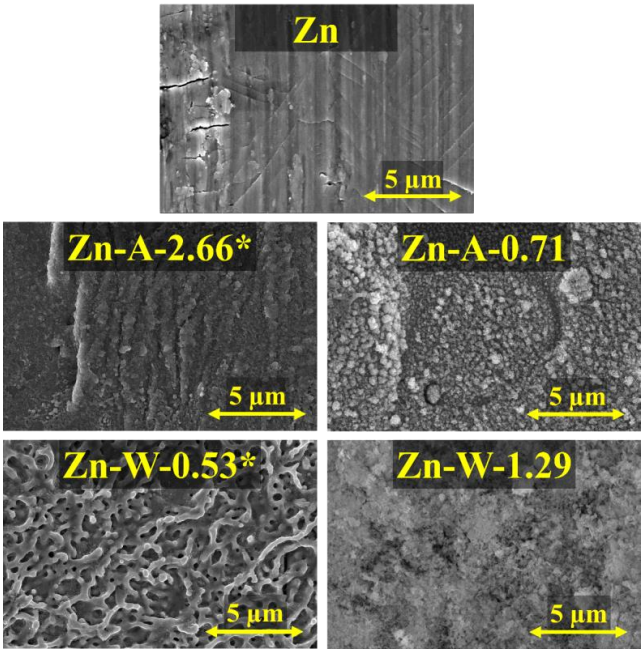

Fig. 3.2. SEM micrographs of untreated and pulsed laser irradiated Zn samples at different energy fluxes (A – in air medium, and W – in water medium).

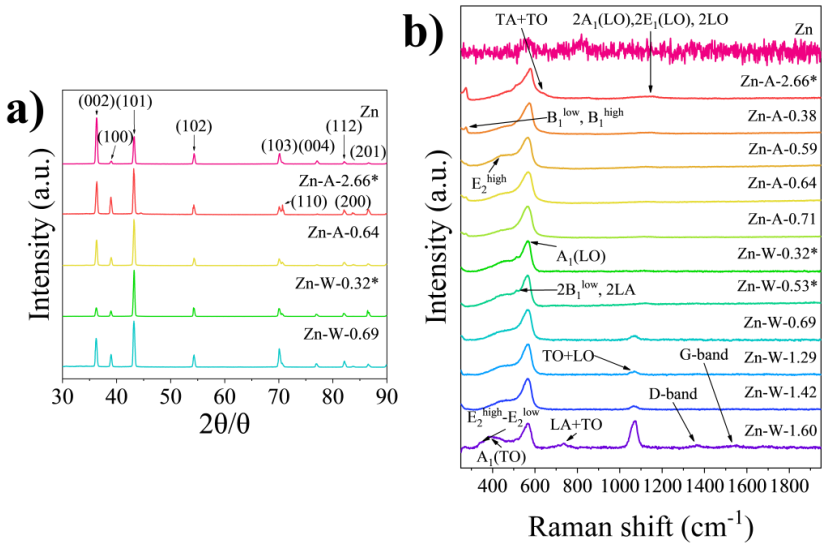

Fig. 3.3. Untreated and laser-irradiated Zn samples: a) XRD diffractograms; b) Raman spectra.

In CV measurements shown in Fig. 3.4 a and b, significant improvements in electrochemical properties are observed for laser-irradiated samples. During anodic oxidation (in accordance with reaction (1)), the Zn sample dissolves electrochemically until the electrolyte can no longer access the active Zn surface for further reaction. During this reaction, $Zn(OH)_4^{2-}$ is formed, which immediately turns into ZnO and covers the anode surface. In turn, during the cathodic reduction reaction, a rapid increase in current is observed at −1.3 V [149], [150]. In this potential region, when ZnO is reduced back to Zn, the previously unreacted Zn surface is exposed to the electrolyte. This appears as a sharp current increase, indicating resumed Zn oxidation. Notably, this phenomenon is less pronounced in laser-treated samples, suggesting that oxidation is more controlled and ZnO grows more uniformly, despite that oxidation is at a higher maximum current. This implies that laser surface treatment improves the overall cyclic performance of the Zn electrode, and treated surfaces show higher oxidation and reduction currents, indicating enhanced reaction kinetics.

Specific surface capacities determined from CV measurements are summarized in Fig. 3.4 c and d. At a scan rate of 0.005 V/s, samples irradiated in air show slightly higher specific surface capacity (1.35–1.50 mAh/cm^2) compared to those irradiated in water (1.25–1.35 mAh/cm^2), and significantly higher than untreated Zn (1.15 mAh/cm^2). Overall, laser-irradiated samples exhibit an 8–30 % increase in capacity depending on the treatment parameters. This increase is attributed to enhanced surface roughness and more active reaction sites caused by laser-induced melting and re-solidification.

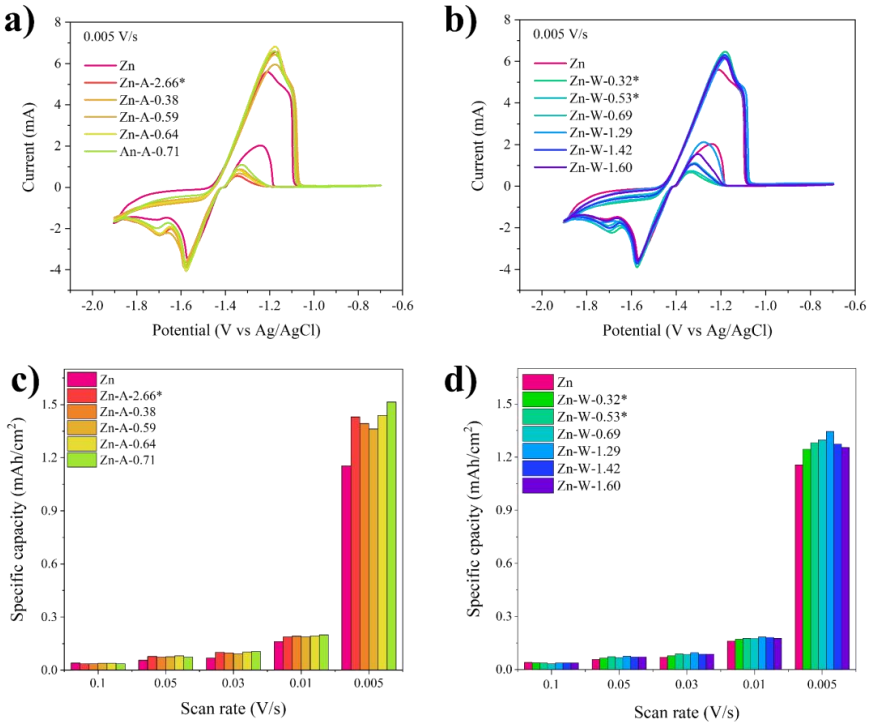

Fig. 3.4. Untreated and air-irradiated Zn samples: a) CV measurements; c) specific surface capacities. Untreated and water-irradiated Zn samples: b) CV measurements; d) specific surface capacities.

After electrochemical measurements, samples were re-examined using SEM (Fig. 3.5) to assess surface changes. The irradiated samples show grain structures with pronounced hexagonal Zn crystal facets. In contrast, the untreated Zn sample surface lacks defined crystal facets and shows random growth features.

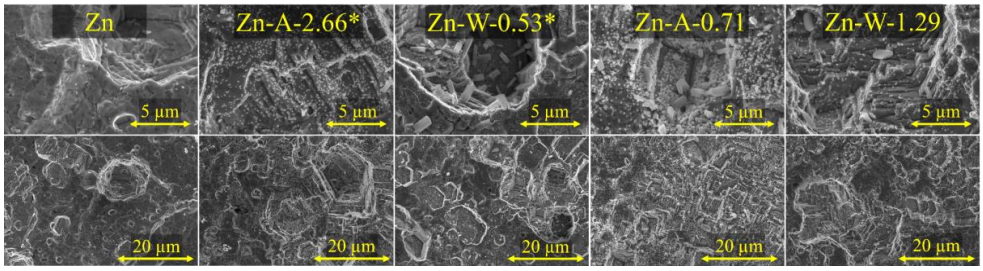

Fig. 3.5. SEM micrographs of untreated and laser-irradiated Zn samples after CV measurements.

Raman spectra of irradiated samples after electrochemical measurements, shown in Fig. 3.6 a, exhibit increased background, and characteristic ZnO peaks are difficult to identify. Conversely, untreated Zn samples still display ZnO peaks at 382 cm^{-1}, 441 cm^{-1} and 585 cm^{-1}, indicating that laser treatment improves Zn anode electrochemical reactions by promoting more uniform ZnO growth and more complete reversion to metallic Zn. However, untreated Zn samples only undergo partial charging (ZnO reduction to Zn), leading to increased ZnO content and a stronger ZnO Raman signal. This observation correlates with CV results of untreated Zn (Fig. 3.4 a and b), which show a more pronounced phenomenon at −1.3 V, linked to increased ZnO formation on the surface.

XRD (Theta/2theta) diffractograms were also repeatedly taken for the sample surfaces after CV measurements, which are shown in Fig. 3.6 b. The untreated Zn sample shows increased intensity of the (002) plane and reduced intensity of the (101) plane, indicating preferential growth in the (002) direction. A slight increase in the (100) plane suggests dendrite-like and porous structure formation [151]. In contrast, irradiated samples retain a polycrystalline (101) structure after CV. An increase in the (002) c-plane direction suggests a more horizontal structure formation. A slight decrease in (100) and (200) plane intensities indicates better resistance to dendrite formation. As illustrated schematically in Fig. 3.6 c, the growth directions of characteristic Zn planes influence potential surface structures. Growth in the (002) plane corresponds to smooth horizontal structures, while growth in (110) and (100) planes indicates dendritic and porous structures.

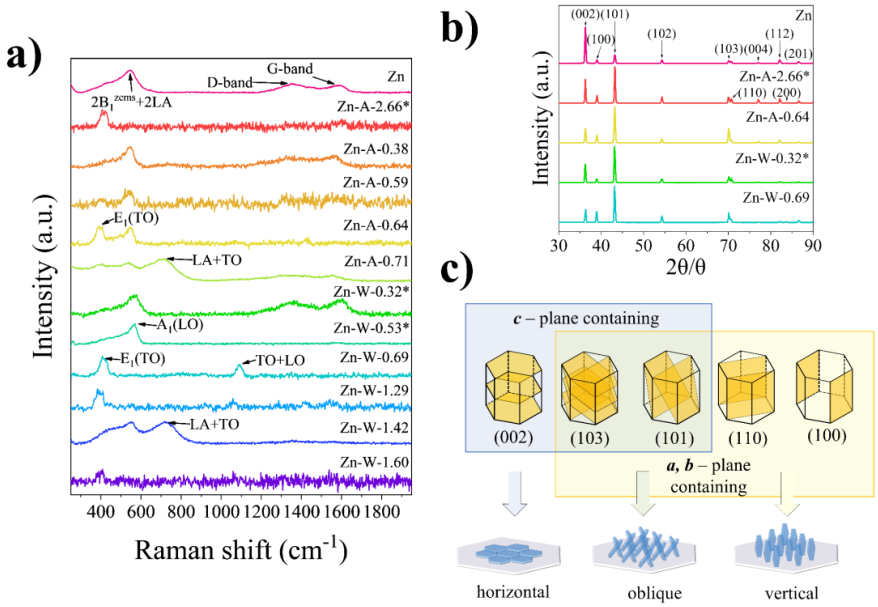

Fig. 3.6. Post-CV measurement results for untreated and laser-irradiated Zn samples: a) Raman spectra; b) XRD diffractograms; c) schematic of hexagonal Zn characteristic crystal planes and growth models.

To further characterize the electrode-electrolyte interface, EIS analysis was performed. EIS spectra at a negative DC offset of –150 mV from OCV are shown in Fig. 3.7 a, and spectra at a positive offset of +150 mV from OCV are in Fig. 3.7 b. Additionally, EIS spectra were fitted using equivalent circuits shown in the graphs, and component values are summarized in Table 3.2. At negative voltage, resistance R_1 is about 27 Ω for all samples, corresponding to the ohmic resistance of the electrolyte. Resistance R_2 represents the charge transfer resistance of the faradaic process and is lower for laser-treated samples. However, CPE value (representing the double-layer capacitance) is increased for irradiated samples, indicating a macroscopically increased surface area. At low frequencies, all spectra transition into a sloped line, corresponding to Warburg impedance related to diffusion-limited processes.

An extended equivalent circuit model was applied to the obtained EIS diagrams at a positive voltage bias, where Zn oxidation and ZnO formation occur. As before, R_s represents the electrolyte resistance and is about 27 Ω. The first R_1 and CPE_1 parallel connection characterizes the state of the electric double layer: R_1 is the ion polarization resistance, and CPE_1 is the double-layer capacitance. Capacitance values are similar, indicating that the macro-surface does not change during the electrochemical reaction. The second parallel circuit of CPE_2 and R_2 describes the faradaic process, where R_2 corresponds to charge transfer resistance. For untreated Zn, this value is 38 Ω; however, for laser-treated samples, it increases to about 200 Ω. This increase is associated with laser-induced defects, also observed in Raman spectra after electrochemical measurements (Fig. 3.6 a). This increases the charge transfer resistance in the irradiated samples and reduces the reaction rate for Zn oxidation. CPE_2 reflects the Zn oxidation process capacitance and is several orders of magnitude higher than the double-layer capacitance. This decrease in capacitance is related to the slowed reaction due to the increased resistance of irradiated samples.

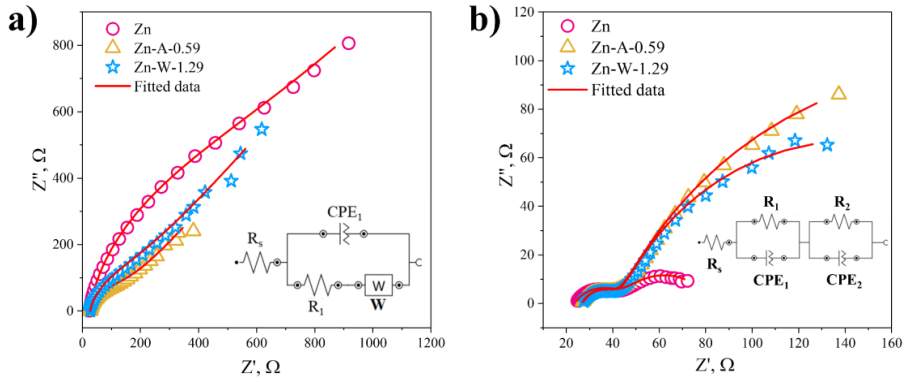

Fig. 3.7. EIS spectra of untreated and laser-irradiated Zn samples: a) at −150 mV DC offset from OCV; b) at +150 mV DC offset from OCV.

Table 3.2

Parameters of the Equivalent Circuit of EIS Fitted Data

Sample	R_s	R_1	CPE_1		R_2	CPE_2	
			Y^0	N		Y^0	N
	Ω	Ω	$\mu S \cdot s^N$		Ω	$\mu S \cdot s^N$	
at a negative DC offset from OCV							
Zn	24.7	668	70	0.90	–	–	–
Zn-A-0.59	26.5	185	103	0.87	–	–	–
Zn-W-1.29	26.5	132	124	0.84	–	–	–
at a positive DC offset from OCV							
Zn	23.6	20.5	369	0.63	38	6.35	0.67
Zn-A-0.59	26.7	15.5	292	0.70	304	3.95	0.72
Zn-W-1.29	27.0	16.0	290	0.70	200	3.79	0.72

4. Main results about the development of amphoteric batteries using hydrogels with different pH environments

This chapter describes the development of an innovatively designed aqueous Zn-MnO_2 battery and the evaluation of its electrochemical properties. The basis of this innovative design is an elevated OCV above that of the commercially available 1.5 V alkaline Zn-MnO_2 battery. This is achieved without the use of membranes, utilizing hydrogel electrolytes with differing pH environments, where the Zn anode is located in an alkaline (KOH) hydrogel electrolyte and the MnO_2 cathode in an acidic (H_2SO_4) electrolyte. Additionally, the use of a neutral (K_2SO_4) hydrogel as an interfacial layer between the two electrolytes is evaluated. This dual-environment approach minimizes unwanted side reactions, such as Zn anode corrosion in acidic electrolyte and the formation of electrochemically inactive Mn compounds in alkaline electrolyte.

4.1. Methodology

For battery fabrication, 30 wt% Pluronic F-127 micellar solutions were used as electrolytes, dissolved respectively in acidic (0.5 M H_2SO_4), alkaline (1 M KOH) and neutral salt (0.5 M K_2SO_4) solutions. pH indicators were added to the electrolyte solutions to allow visual identification of pH changes. A Zn plate of defined diameter was used as the anode. The cathode consisted of carbon felt impregnated with a mixture of MnO_2 (pyrolusite phase) and CB in a 13 : 5 ratio, further mixed with the acidic hydrogel to form a homogeneous mass.

To evaluate the performance of each electrode and its corresponding hydrogel, half-cell measurements were performed, where the cathode or anode was the working electrode, one platinum electrode was the counter electrode, and the other platinum electrode was the reference electrode. Afterwards, the battery was assembled in a syringe body (Fig. 4.1), allowing

observation of electrolyte changes during operation. First, the MnO_2 cathode felt was inserted at the syringe tip, followed by the 0.5 M H_2SO_4 acidic hydrogel, the 0.4–0.6 M K_2SO_4 neutral hydrogel (only for three-layer batteries), the 1 M KOH alkaline hydrogel, and finally the Zn anode, attached to the syringe plunger. In all battery configurations, the total electrolyte volume was fixed at 3 mL.

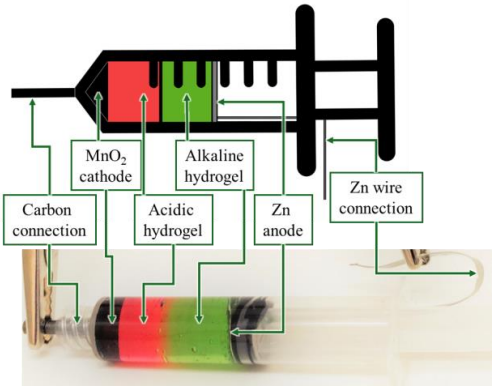

Fig. 4.1. Schematic and photograph of the constructed battery with labelled components.

4.2. Results

To determine the theoretical behaviour of the cathode and anode during battery operation, half-cell CV measurements were conducted. The MnO_2 cathode half-cell with acidic (0.5 M H_2SO_4) hydrogel and Zn anode half-cell with alkaline (1 M KOH) hydrogel were tested against a Pt counter electrode and Pt reference electrode. According to the combined data shown in Fig. 4.2 a, the OCV of the amphoteric battery is approximately 2.3 V. Measurements from several assembled Zn-MnO_2 amphoteric batteries (Fig. 4.2 a) confirm that the voltage ranges from 2.3 V to 2.4 V.

The expected minimum discharge voltage, based on the combined data, should be around 1.6 V. To assess this theoretical value, a complete discharge of the amphoteric Zn-MnO_2 battery was performed (Fig. 4.2 b) with a discharge current of 10 mA/s. Before discharge, the OCV was 2.4 V, the initial discharge plateau was around 2.0 V, and the end-of-discharge voltage was 1.7 V – consistent with observations from the half-cell CV measurements. Additionally, under a lower discharge current of 0.1 mA/s (Fig. 4.2 c), the initial voltage was 2.34 V, decreasing to 2.2 V over 10 hours.

During all measurements, the formation of a visibly neutral pH layer between the two hydrogels was observed. This can be explained by H^+ and OH^- ion diffusion from the acidic and alkaline electrolytes, where they neutralize in the interface, forming water, further diluting both hydrogel electrolytes and increasing internal resistance. To assess the influence of this neutral layer, OCV measurements were also carried out using an additional neutral hydrogel between the acidic and alkaline layers. The neutral electrolyte concentration (K_2SO_4) was varied relative to the acid/base concentration at 0.4 M, 0.5 M, and 0.6 M. According to the

measurements shown in Fig. 4.2 d, three-layer hydrogel electrolyte batteries maintained a stable voltage for over 45 h – longer than two-layer batteries, which dropped to 1.7 V after ~ 27 h due to the neutralization reaction. Among the three concentrations, the balanced 0.5 M hydrogel exhibited the longest voltage stability (~ 52 h), while both the lower and higher concentrations maintained stability only up to ~ 45 h. Overall, the pH gradient stability of the three-layer hydrogel electrolyte battery is more pronounced than that of the two-layer system.

To evaluate internal resistances, EIS measurements were performed on a fully assembled amphoteric Zn-MnO_2 battery, and the fitted data according to the equivalent circuit are shown in Fig. 4.3. The obtained parameter values are summarized in Table 4.1. The series resistance R_s of 30.5 Ω corresponds to the electrolyte resistance and is relatively high due to limited ion mobility hindered by micellar structures. The first semicircle at high frequencies represents the electrolyte-electrode interface, which is noted in the equivalent circuit as R_1 and CPE_1 parallel connection. Fitted R_1 was found to be 17 Ω, and the equivalent capacitance of CPE_1 is 102 mF. Both these parameters are sensitive to electrolyte composition [152] and electrode surface porosity [153], [154]. The second semicircle at low frequencies reflects charge-transfer processes, where R_{ct} is the charge transfer resistance with a fitted value of 6.7 Ω, and CPE_2 represents the double-layer capacitance with a fitted value of 39 mF.

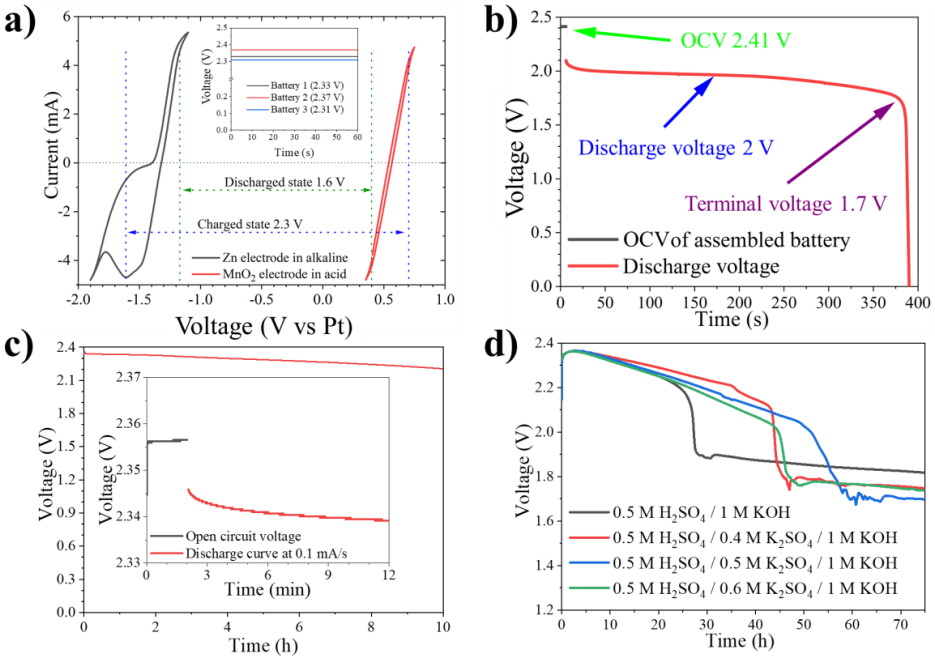

Fig. 4.2. Properties of the amphoteric battery: a) CV measurements of the half-cells in corresponding electrolytes (scan rate 0.01 V/s) and OCV measurements of the prepared batteries; b) OCV and discharge voltage at 10 mA/s discharge current; c) OCV and discharge voltage at 0.1 mA/s; d) OCV measurements for two-layer and three-layer electrolyte batteries with varying neutral layer concentrations.

Table 4.1

Fitted Parameter Values from EIS Measurements Based on the Equivalent Circuit

Parameter	Value	Error, %
R_s	30.5 Ω	0.2
R_1	17.2 Ω	6
CPE_1	106 mF	3
R_{ct}	6.7 Ω	7
CPE_2	39 mF	4

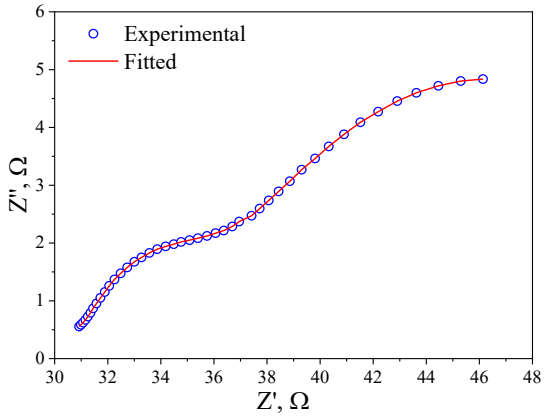

Fig. 4.3. EIS spectrum with fitted model and equivalent circuit.

Chronopotentiometry results for the amphoteric Zn-MnO_2 rechargeable battery with two-layer hydrogels (1 M KOH and 0.5 M H_2SO_4) are shown in Fig. 4.4 a, and OCV measurements before discharge, after 100 cycles, and after 200 cycles are shown in Fig. 4.4 b. The upper charge voltage of the battery was around 2.7 V, and the lowest discharge voltage ranged from 2.2–2.3 V. Additional OCV measurements show that the voltage of 2.34 V remained stable throughout 14 hours of cycling. During the measurements, ion diffusion was observed with a visible formation of a neutral pH layer between the hydrogels due to H^+ and OH^- ion migration and their neutralization, forming water. This further diluted both electrolytes, increasing internal resistance. Additionally, K^+ and SO_4^{2-} ions (counterions of the base and acid, respectively, and responsible for ion conductivity) also migrated toward the battery centre, forming crystalline potassium sulphate. This is explained by the limited solubility of K_2SO_4 in water (120 g/L at 25 °C), further contributing to internal resistance.

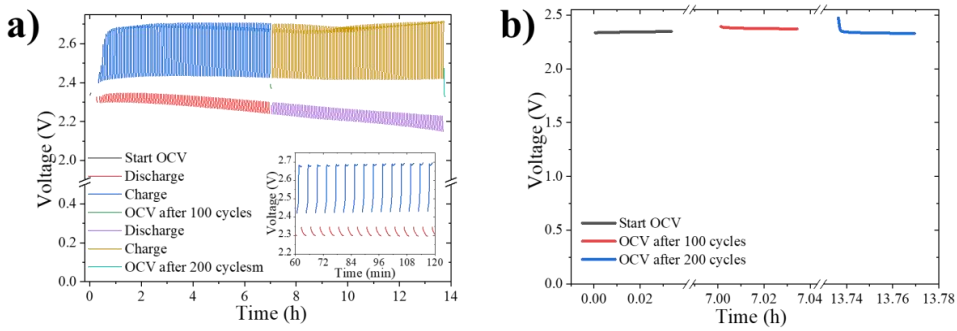

Fig. 4.4. Chronopotentiometry of the two-layer (acidic and alkaline) hydrogel Zn-MnO_2 amphoteric battery: a) charge/discharge curves; and b) OCV before discharge, after 100 and 200 charge/discharge cycles. Charge-discharge current: +/– 1 mA/s.

To assess the effect of the neutral layer in the battery structure, additional chronopotentiometry and OCV measurements were conducted for batteries with a three-layer electrolyte – 1 M KOH, 0.5 M K_2SO_4 and 0.5 M H_2SO_4 – shown in Fig. 4.5 a and b. The charge voltage of the three-layer hydrogel battery was 0.5 V higher, and the discharge voltage was 0.5 V lower than in the two-layer battery (Fig. 4.4 a). This charge/discharge voltage discrepancy is due to the higher resistance of the hydrogel electrolyte in the three-layer configuration. While the conductivity of the acidic (0.5 M H_2SO_4) hydrogel is 83.6 mS/cm (at 23 °C) and the basic (1 M KOH) hydrogel is 78.6 mS/cm (at 23 °C), the neutral (0.5 M K_2SO_4) hydrogel conductivity is more than 6 times lower – 12.6 mS/cm (at 23 °C). This results in a significantly higher total resistance in the three-layer system, causing the observed charge–discharge voltage mismatch. However, the OCV of 2.32 V for the three-layer hydrogel battery (Fig. 4.5 b) remained stable, similarly to the two-layer battery (Fig. 4.4 b).

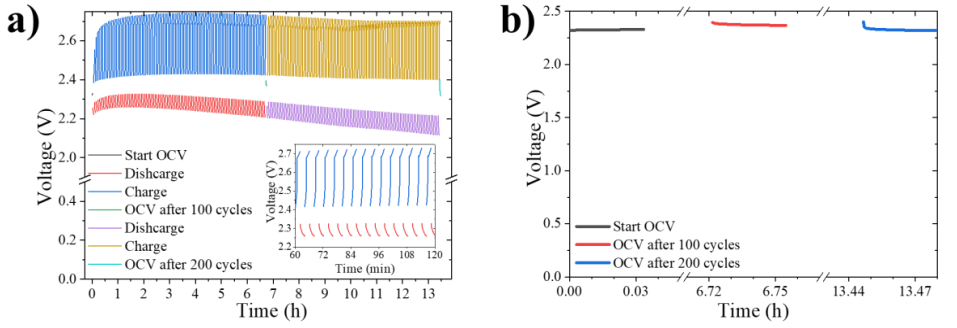

Fig. 4.5. Chronopotentiometry of the three-layer (acidic, neutral, alkaline) hydrogel Zn-MnO_2 amphoteric battery: a) charge/discharge curves; and b) OCV before discharge, after 100 and 200 charge/discharge cycles. Charge–discharge current: +/– 1 mA/s.

CONCLUSIONS

1. Using a pH gradient electrolyte system, where the Zn anode operates in an alkaline environment, and the MnO_2 cathode operates in an acidic environment, shifts the hydrogen evolution reaction to a lower potential (to –0.81 V) and the oxygen evolution reaction to a higher potential (to +1.2 V), increasing the electrochemical window of water.
2. By doping the MnO_2 cathode with Bi^{3+} and Mo^{6+} ions, Mn^{3+} ions are stabilized in the material, which promotes the formation of the electrochemically more active α-MnO_2 phase structure. The optimal concentrations have been determined: 5–10 mol% Bi and 2.5 mol% Mo.
3. Irradiating the Zn anode with a pulsed laser increases the specific surface capacity by 30 % and reduces the charge transfer resistance, which improves the kinetics of the electrochemical reaction in a 1 M KOH electrolyte solution.
4. Using Pluronic F-127 micelle hydrogels, a rechargeable amphoteric aqueous electrolyte Zn-MnO_2 battery is obtained, where the Zn anode is in a 1 M KOH electrolyte solution, and the MnO_2 cathode is in a 0.5 M H_2SO_4 electrolyte solution.
5. The open-circuit voltage of the amphoteric aqueous electrolyte Zn-MnO_2 battery is 2.4 V, the pH gradient stability is maintained for more than 25 hours, the discharge voltage at 0.1 mA/s is 2.34 V, and it is stable for 200 charge–discharge cycles at 1 mA/s.

REFERENCES

[1] J. L. Holechek, H. M. E. Geli, M. N. Sawalhah, R. Valdez. A Global Assessment: Can Renewable Energy Replace Fossil Fuels by 2050? Sustainability, 14 (2022), 4792. https://doi.org/10.3390/su14084792.

[2] Q. Jiang, S. I. Khattak, M. Ahmad, P. Lin. Mitigation pathways to sustainable production and consumption: Examining the impact of commercial policy on carbon dioxide emissions in Australia, Sustain. Prod. Consum., 25 (2021), 390–403. https://doi.org/10.1016/j.spc.2020.11.016.

[3] T.-Y. Chen, C.-J. Huang. A Two-Tier Scenario Planning Model of Environmental Sustainability Policy in Taiwan, Sustainability, 11 (2019), 2336. https://doi.org/10.3390/su11082336.

[4] I. Kougias, N. Taylor, G. Kakoulaki, A. Jäger-Waldau. The role of photovoltaics for the European Green Deal and the recovery plan, Renewable and Sustainable Energy Reviews, 144 (2021), 111017. https://doi.org/10.1016/j.rser.2021.111017.

[5] S. García-Freites, C. Gough, M. Röder. The greenhouse gas removal potential of bioenergy with carbon capture and storage (BECCS) to support the UK's net-zero emission target, Biomass Bioenergy, 151 (2021), 106164. https://doi.org/10.1016/j.biombioe.2021.106164.

[6] J. Collins, G. Gourdin, D. Qu. Modern Applications of Green Chemistry, in: Green Chemistry, Elsevier, 2018: pp. 771–860. https://doi.org/10.1016/B978-0-12-809270-5.00028-5.

[7] T. Placke, R. Kloepsch, S. Dühnen, M. Winter. Lithium ion, lithium metal, and alternative rechargeable battery technologies: the odyssey for high energy density, Journal of Solid State Electrochemistry, 21 (2017), 1939–1964. https://doi.org/10.1007/s10008-017-3610-7.

[8] Y. Sui, C. Liu, R. C. Masse, Z. G. Neale, M. Atif, M. AlSalhi, G. Cao. Dual-ion batteries: The emerging alternative rechargeable batteries, Energy Storage Mater., 25 (2020), 1–32. https://doi.org/10.1016/j.ensm.2019.11.003.

[9] M. S. Ziegler, J. M. Mueller, G. D. Pereira, J. Song, M. Ferrara, Y.-M. Chiang, J. E. Trancik. Storage Requirements and Costs of Shaping Renewable Energy Toward Grid Decarbonization, Joule, 3 (2019), 2134–2153. https://doi.org/10.1016/j.joule.2019.06.012.

[10] J. Y. Lee, A. K. Ramasamy, K. H. Ong, R. Verayiah, H. Mokhlis, M. Marsadek. Energy storage systems: A review of its progress and outlook, potential benefits, barriers and solutions within the Malaysian distribution network, J. Energy Storage, 72 (2023), 108360. https://doi.org/10.1016/j.est.2023.108360.

[11] T.-Z. Ang, M. Salem, M. Kamarol, H. S. Das, M. A. Nazari, N. Prabaharan. A comprehensive study of renewable energy sources: Classifications, challenges and suggestions, Energy Strategy Reviews, 43 (2022), 100939. https://doi.org/10.1016/j.esr.2022.100939.

[12] J. Escudero-González, P. A. López-Jiménez. Iron redox battery as electrical energy storage system in the Spanish energetic framework, International Journal of Electrical Power & Energy Systems, 61 (2014), 421–428. https://doi.org/10.1016/j.ijepes.2014.03.067.

[13] L. Kong, C. Li, J. Jiang, M. G. Pecht. Li-Ion Battery Fire Hazards and Safety Strategies, Energies (Basel), 11 (2018), 2191. https://doi.org/10.3390/en11092191.

[14] Y. Liu, Y. Liu, B. Zhu, Z. Wang, X. Zhang, X. Wu. Multilayer Ti3C2Tx-loaded CoOHF composite structures for high-performance lithium-ion batteries, Mater. Res. Bull., 179 (2024), 112986. https://doi.org/10.1016/j.materresbull.2024.112986.

[15] S. Siriroj, J. Padchasri, A. Montreeuppathum, S. Sonsupap, S. Maensiri, S. Kheawhom, P. Kidkhunthod. Glass-sulfur composite cathodes: A new strategy for improving the performance of lithium-sulfur batteries, Mater. Res. Bull., 178 (2024), 112919. https://doi.org/10.1016/j.materresbull.2024.112919.

[16] S. Xu, S. Liu, Y. Zhou, R. Xiao, X. Ke. Study on the electrochemical process of Li+/Na+ mixed organic dual-cation battery system, Mater. Res. Bull., 177 (2024), 112858. https://doi.org/10.1016/j.materresbull.2024.112858.

[17] J. Wu, Y. Cao, H. Zhao, J. Mao, Z. Guo. The critical role of carbon in marrying silicon and graphite anodes for high-energy lithium-ion batteries, Carbon Energy, 1 (2019), 57–76. https://doi.org/10.1002/cey2.2.

[18] J. Yang, X. Liu, J. Tian, X. Ma, B. Wang, W. Li, Q. Wang. Adhesive nanocomposites of hypergravity-induced Co3O4 nanoparticles and natural gels as Li-ion battery anode materials with high capacitance and low resistance, RSC Adv., 7 (2017), 21061–21067. https://doi.org/10.1039/c7ra02725g.

[19] M. B. Lim, T. N. Lambert, B. R. Chalamala. Rechargeable alkaline zinc–manganese oxide batteries for grid storage: Mechanisms, challenges and developments, Materials Science and Engineering: R: Reports, 143 (2021), 100593. https://doi.org/10.1016/j.mser.2020.100593.

[20] J. Park, M. Kim, J. Choi, S. Lee, J. Kim, D. Han, H. Jang, M. Park. Recent Progress in High-voltage Aqueous Zinc-based Hybrid Redox Flow Batteries, Chem. Asian J., 18 (2023). https://doi.org/10.1002/asia.202201052.

[21] W. M. Seong, K.-Y. Park, M. H. Lee, S. Moon, K. Oh, H. Park, S. Lee, K. Kang. Abnormal self-discharge in lithium-ion batteries, Energy Environ. Sci., 11 (2018), 970–978. https://doi.org/10.1039/C8EE00186C.

[22] T. Or, S. W. D. Gourley, K. Kaliyappan, A. Yu, Z. Chen. Recycling of mixed cathode lithium-ion batteries for electric vehicles: Current status and future outlook, Carbon Energy, 2 (2020), 6–43. https://doi.org/10.1002/cey2.29.

[23] H. Wang, Y. Liu, Y. Li, Y. Cui. Lithium Metal Anode Materials Design: Interphase and Host, Electrochemical Energy Reviews, 2 (2019), 509–517. https://doi.org/10.1007/s41918-019-00054-2.

[24] W. Xu, J. Wang, F. Ding, X. Chen, E. Nasybulin, Y. Zhang, J.-G. Zhang. Lithium metal anodes for rechargeable batteries, Energy Environ. Sci., 7 (2014), 513–537. https://doi.org/10.1039/C3EE40795K.

[25] Y. S. Duh, K. H. Lin, C. S. Kao, Experimental investigation and visualization on thermal runaway of hard prismatic lithium-ion batteries used in smart phones, J. Therm. Anal. Calorim., 132 (2018), 1677–1692. https://doi.org/10.1007/s10973-018-7077-2.

[26] N. Nitta, F. Wu, J. T. Lee, G. Yushin. Li-ion battery materials: Present and future, Materials Today, 18 (2015), 252–264. https://doi.org/10.1016/j.mattod.2014.10.040.

[27] W. Zaman, K. B. Hatzell, Processing and manufacturing of next-generation lithium-based all-solid-state batteries, Curr. Opin. Solid. State Mater. Sci., 26 (2022), 101003. https://doi.org/10.1016/j.cossms.2022.101003.

[28] H. Wang, W. Shi, F. Hu, Y. Wang, X. Hu, H. Li. Over-heating triggered thermal runaway behavior for lithium-ion battery with high nickel content in positive electrode, Energy, 224 (2021). https://doi.org/10.1016/j.energy.2021.120072.

[29] S. Chen, Z. Gao, T. Sun. Safety challenges and safety measures of Li-ion batteries, Energy Sci. Eng., 9 (2021), 1647–1672. https://doi.org/10.1002/ese3.895.

[30] A. Zeng, W. Chen, K. D. Rasmussen, X. Zhu, M. Lundhaug, D. B. Müller, J. Tan, J. K. Keiding, L. Liu, T. Dai, A. Wang, G. Liu. Battery technology and recycling alone will not save the electric mobility transition from future cobalt shortages, Nat. Commun., 13 (2022). https://doi.org/10.1038/s41467-022-29022-z.

[31] J. Zhang, Y. Lei, Z. Lin, P. Xie, H. Lu, J. Xu. A novel approach to recovery of lithium element and production of holey graphene based on the lithiated graphite of spent lithium ion batteries, Chemical Engineering Journal, 436 (2022). https://doi.org/10.1016/j.cej.2022.135011.

[32] B. Liu, Q. Zhang, J. Liu, Y. Hao, Y. Tang, Y. Li. The impacts of critical metal shortage on China's electric vehicle industry development and countermeasure policies, Energy, 248 (2022). https://doi.org/10.1016/j.energy.2022.123646.

[33] T. Wu, W. Zhang, J. Yang, Q. Lu, J. Peng, M. Zheng, F. Xu, Y. Liu, Y. Liang. Architecture engineering of carbonaceous anodes for high-rate potassium-ion batteries, Carbon Energy, 3 (2021), 554–581. https://doi.org/10.1002/cey2.99.

[34] M. Minakshi, D. R. G. Mitchell. The influence of bismuth oxide doping on the rechargeability of aqueous cells using MnO2 cathode and LiOH electrolyte, Electrochim. Acta, 53 (2008), 6323–6327. https://doi.org/10.1016/j.electacta.2008.04.013.

[35] N. Zhang, F. Cheng, J. Liu, L. Wang, X. Long, X. Liu, F. Li, J. Chen. Rechargeable aqueous zinc-manganese dioxide batteries with high energy and power densities, Nat. Commun., 8 (2017), 405. https://doi.org/10.1038/s41467-017-00467-x.

[36] H. Zhang, W. Lu, X. Li. Progress and Perspectives of Flow Battery Technologies, Electrochemical Energy Reviews, 2 (2019), 492–506. https://doi.org/10.1007/s41918-019-00047-1.

[37] H. Luo, B. Liu, Z. Yang, Y. Wan, C. Zhong. The Trade-Offs in the Design of Reversible Zinc Anodes for Secondary Alkaline Batteries, Electrochemical Energy Reviews, 5 (2022), 187–210. https://doi.org/10.1007/s41918-021-00107-5.

[38] G. G. Yadav, X. Wei, J. Huang, D. Turney, M. Nyce, S. Banerjee, Accessing the second electron capacity of MnO2 by exploring complexation and intercalation reactions in

energy dense alkaline batteries, Int. J. Hydrogen Energy, 43 (2018), 8480–8487. https://doi.org/10.1016/j.ijhydene.2018.03.061.

[39] Y. Liao, H.-C. Chen, C. Yang, R. Liu, Z. Peng, H. Cao, K. Wang. Unveiling performance evolution mechanisms of MnO2 polymorphs for durable aqueous zinc-ion batteries, Energy Storage Mater., 44 (2022), 508–516. https://doi.org/10.1016/j.ensm.2021.10.039.

[40] S. Yao, R. Zhao, S. Wang, Y. Zhou, R. Liu, L. Hu, A. Zhang, R. Yang, X. Liu, Z. Fu, D. Wang, Z. Yang, Y.-M. Yan. Ni-doping induced structure distortion of MnO2 for highly efficient Na+ storage, Chemical Engineering Journal, 429 (2022), 132521. https://doi.org/10.1016/j.cej.2021.132521.

[41] X. Zhang, J. Hu, N. Fu, W. Zhou, B. Liu, Q. Deng, X. Wu. Comprehensive review on <scp>zinc-ion</scp> battery anode: Challenges and strategies, Info. Mat., 4 (2022). https://doi.org/10.1002/inf2.12306.

[42] C. Nie, G. Wang, D. Wang, M. Wang, X. Gao, Z. Bai, N. Wang, J. Yang, Z. Xing, S. Dou. Recent Progress on Zn Anodes for Advanced Aqueous Zinc-Ion Batteries, Adv. Energy Mater., 13 (2023). https://doi.org/10.1002/aenm.202300606.

[43] C. Zhu, P. Li, G. Xu, H. Cheng, G. Gao. Recent progress and challenges of Zn anode modification materials in aqueous Zn-ion batteries, Coord. Chem., Rev. 485 (2023), 215142. https://doi.org/10.1016/j.ccr.2023.215142.

[44] Y. Xie, Y. Yu, X. Gong, Y. Guo, Y. Guo, Y. Wang, G. Lu. Effect of the crystal plane figure on the catalytic performance of MnO_2 for the total oxidation of propane, Cryst. Eng. Comm., 17 (2015), 3005–3014. https://doi.org/10.1039/C5CE00058K.

[45] S. Jana, S. Basu, S. Pande, S. K. Ghosh, T. Pal. Shape-Selective Synthesis, Magnetic Properties, and Catalytic Activity of Single Crystalline β-MnO_2 Nanoparticles, The Journal of Physical Chemistry C, 111 (2007), 16272–16277. https://doi.org/10.1021/jp074803l.

[46] J. K. Seo, J. Shin, H. Chung, P. Y. Meng, X. Wang, Y. S. Meng. Intercalation and Conversion Reactions of Nanosized β-MnO_2 Cathode in the Secondary Zn/MnO_2 Alkaline Battery, The Journal of Physical Chemistry C, 122 (2018), 11177–11185. https://doi.org/10.1021/acs.jpcc.7b11685.

[47] H.-W. Zhu, J. Ge, Y.-C. Peng, H.-Y. Zhao, L.-A. Shi, S.-H. Yu. Dip-coating processed sponge-based electrodes for stretchable Zn-MnO_2 batteries, Nano Res., 11 (2018), 1554–1562. https://doi.org/10.1007/s12274-017-1771-4.

[48] X. Guo, J. Zhou, C. Bai, X. Li, G. Fang, S. Liang, Zn/MnO_2 battery chemistry with dissolution-deposition mechanism, Mater. Today Energy, 16 (2020), 100396. https://doi.org/10.1016/j.mtener.2020.100396.

[49] L. Wu, Z. Li, Y. Xiang, W. Dong, X. Qi, Z. Ling, Y. Xu, H. Wu, M. D. Levi, N. Shpigel, X. Zhang. Revisiting the Charging Mechanism of α-MnO_2 in Mildly Acidic Aqueous Zinc Electrolytes, Small 20 (2024). https://doi.org/10.1002/smll.202404583.

[50] H. Chen, C. Dai, F. Xiao, Q. Yang, S. Cai, M. Xu, H. J. Fan, S. Bao. Reunderstanding the Reaction Mechanism of Aqueous Zn-Mn Batteries with Sulfate Electrolytes: Role of

the Zinc Sulfate Hydroxide, Advanced Materials, 34 (2022). https://doi.org/10.1002/adma.202109092.

[51] L. Li, T. K. A. Hoang, J. Zhi, M. Han, S. Li, P. Chen. Functioning Mechanism of the Secondary Aqueous Zn-β-MnO_2 Battery, ACS Appl. Mater. Interfaces., 12 (2020), 12834–12846. https://doi.org/10.1021/acsami.9b22758.

[52] D. Chao, W. Zhou, C. Ye, Q. Zhang, Y. Chen, L. Gu, K. Davey, S. Qiao. An Electrolytic Zn-MnO_2 Battery for High-Voltage and Scalable Energy Storage, Angewandte Chemie International Edition, 58 (2019), 7823–7828. https://doi.org/10.1002/anie.201904174.

[53] S. J. Kim, D. Wu, L. M. Housel, L. Wu, K. J. Takeuchi, A. C. Marschilok, E. S. Takeuchi, Y. Zhu, Toward the Understanding of the Reaction Mechanism of Zn/MnO_2 Batteries Using Non-alkaline Aqueous Electrolytes, Chemistry of Materials, 33 (2021), 7283–7289. https://doi.org/10.1021/acs.chemmater.1c01542.

[54] C. Zhong, B. Liu, J. Ding, X. Liu, Y. Zhong, Y. Li, C. Sun, X. Han, Y. Deng, N. Zhao, W. Hu. Decoupling electrolytes towards stable and high-energy rechargeable aqueous zinc–manganese dioxide batteries, Nat. Energy, 5 (2020), 440–449. https://doi.org/10.1038/s41560-020-0584-y.

[55] S. Hasegawa, K. Shimotani, K. Kishi, H. Watanabe. Electricity Generation from Decomposition of Hydrogen Peroxide, Electrochemical and Solid-State Letters, 8 (2005), A119. https://doi.org/10.1149/1.1849112.

[56] J. L. Cohen, D. J. Volpe, D. A. Westly, A. Pechenik, H. D. Abruña. A Dual Electrolyte H_2/O_2 Planar Membraneless Microchannel Fuel Cell System with Open Circuit Potentials in Excess of 1.4 V, Langmuir, 21 (2005), 3544–3550. https://doi.org/10.1021/la0479307.

[57] E. R. Choban, J. S. Spendelow, L. Gancs, A. Wieckowski, P. J. A. Kenis. Membraneless laminar flow-based micro fuel cells operating in alkaline, acidic, and acidic/alkaline media, Electrochim. Acta, 50 (2005), 5390–5398. https://doi.org/10.1016/j.electacta.2005.03.019.

[58] G. G. Yadav, D. Turney, J. Huang, X. Wei, S. Banerjee. Breaking the 2 V Barrier in Aqueous Zinc Chemistry: Creating 2.45 and 2.8 V MnO_2 –Zn Aqueous Batteries, ACS Energy Lett., 4 (2019), 2144–2146. https://doi.org/10.1021/acsenergylett.9b01643.

[59] C. Liu, X. Chi, Q. Han, Y. Liu,.A High Energy Density Aqueous Battery Achieved by Dual Dissolution/Deposition Reactions Separated in Acid-Alkaline Electrolyte, Adv. Energy Mater., 10 (2020), 1903589. https://doi.org/10.1002/aenm.201903589.

[60] J. Liu, J. Bao, X. Zhang, Y. Gao, Y. Zhang, L. Liu, Z. Cao. MnO_2 -based materials for supercapacitor electrodes: challenges, strategies and prospects, RSC Adv., 12 (2022), 35556–35578. https://doi.org/10.1039/D2RA06664E.

[61] S. Devaraj, N. Munichandraiah. Effect of Crystallographic Structure of MnO_2 on Its Electrochemical Capacitance Properties, The Journal of Physical Chemistry C, 112 (2008), 4406–4417. https://doi.org/10.1021/jp7108785.

[62] B. Yin, S. Zhang, H. Jiang, F. Qu, X. Wu. Phase-controlled synthesis of polymorphic MnO_2 structures for electrochemical energy storage, J. Mater. Chem. A Mater., 3 (2015), 5722–5729. https://doi.org/10.1039/C4TA06943A.

[63] Z. Zhang, W. Li, Y. Shen, R. Wang, H. Li, M. Zhou, W. Wang, K. Wang, K. Jiang. Issues and opportunities of manganese-based materials for enhanced Zn-ion storage performances, J. Energy Storage, 45 (2022), 103729. https://doi.org/10.1016/j.est.2021.103729.

[64] C. Chen, M. Shi, Y. Zhao, C. Yang, L. Zhao, C. Yan. Al-Intercalated MnO_2 cathode with reversible phase transition for aqueous Zn-Ion batteries, Chemical Engineering Journal, 422 (2021), 130375. https://doi.org/10.1016/j.cej.2021.130375.

[65] J. Yao, J. Ji, H. Wan, J. Duan, X. Wang, L. Lv, G. Ma, L. Tao, H. Wang, J. Zhang, H. Wang. Highly stable Co-doped MnO2 nanoarrays as enhanced cathode materials for aqueous zinc-ion batteries, Oxford Open Energy, 1 (2022). https://doi.org/10.1093/ooenergy/oiab003.

[66] S. Yang, L. Zhang, M. Luo, Y. Cui, J. Wang, D. Zhao, C. Yang, X. Wang, B. Cao. Synergistic combination of a Co-doped σ-MnO_2 cathode with an electrolyte additive for a high-performance aqueous zinc-ion battery, Chem. Phys. Mater., 2 (2023), 77–82. https://doi.org/10.1016/j.chphma.2022.04.007.

[67] S. Liu, J. Wang, Z. Zhou, Y. Li, W. Zhang, C. Wang. Cobalt-doped δ-MnO_2 /CNT composites as cathode material for aqueous zinc-ion batteries, Inorg. Chem. Front., 10 (2023), 5167–5177. https://doi.org/10.1039/D3QI01010D.

[68] X. Xia, Y. Zhao, Y. Zhao, M. Xu, W. Liu, X. Sun. Mo doping provokes two-electron reaction in MnO_2 with ultrahigh capacity for aqueous zinc ion batteries, Nano Res., 16 (2023), 2511–2518. https://doi.org/10.1007/s12274-022-5057-0.

[69] Y. Liu, W. Chen, J. Su, X. Zhao, X. Pan. Inhibition of phase transition from δ-MnO_2 to α-MnO_2 by Mo-doping and the application of Mo-doped MnO_2 in aqueous zinc-ion batteries, Physical Chemistry Chemical Physics, 25 (2023), 30663–30669. https://doi.org/10.1039/D3CP04182D.

[70] Y. Ma, M. Xu, R. Liu, H. Xiao, Y. Liu, X. Wang, Y. Huang, G. Yuan. Molecular tailoring of MnO_2 by bismuth doping to achieve aqueous zinc-ion battery with capacitor-level durability, Energy Storage Mater., 48 (2022), 212–222. https://doi.org/10.1016/j.ensm.2022.03.024.

[71] D. Im, A. Manthiram. Role of Bismuth and Factors Influencing the Formation of Mn[sub 3]O[sub 4] in Rechargeable Alkaline Batteries Based on Bismuth-Containing Manganese Oxides, J. Electrochem. Soc., 150 (2003), A68. https://doi.org/10.1149/1.1524611.

[72] K. Ma, Q. Li, C. Hong, G. Yang, C. Wang. Bi Doping-Enhanced Reversible-Phase Transition of α-MnO_2 Raising the Cycle Capability of Aqueous Zn–Mn Batteries, ACS Appl. Mater. Interfaces, 13 (2021), 55208–55217. https://doi.org/10.1021/acsami.1c17677.

[73] L. Gou, Y. Yang, Y. Zhang, J. Li, X. Fan, D. Li. In situ synthesis of Bi3+-doped δ-MnO_2 cathode to enhance the cycle stability for aqueous zinc-ion batteries, Journal of Solid State Electrochemistry, 27 (2023), 1443–1450. https://doi.org/10.1007/s10008-023-05501-1.

[74] L. Kang, M. Cui, F. Jiang, Y. Gao, H. Luo, J. Liu, W. Liang, C. Zhi. Nanoporous $CaCO_3$ Coatings Enabled Uniform Zn Stripping/Plating for Long-Life Zinc Rechargeable Aqueous Batteries, Adv. Energy Mater., 8 (2018). https://doi.org/10.1002/aenm.201801090.

[75] X. Xie, S. Liang, J. Gao, S. Guo, J. Guo, C. Wang, G. Xu, X. Wu, G. Chen, J. Zhou. Manipulating the ion-transfer kinetics and interface stability for high-performance zinc metal anodes, Energy Environ. Sci., 13 (2020), 503–510. https://doi.org/10.1039/C9EE03545A.

[76] X. Hu, J. Borowiec, Y. Zhu, X. Liu, R. Wu, A. M. Ganose, I. P. Parkin, B. D. Boruah. Dendrite-Free Zinc Anodes Enabled by Exploring Polar-Face-Rich 2D ZnO Interfacial Layers for Rechargeable Zn-Ion Batteries, Small, 20 (2024). https://doi.org/10.1002/smll.202306827.

[77] Q. Ren, X. Tang, K. He, C. Zhang, W. Wang, Y. Guo, Z. Zhu, X. Xiao, S. Wang, J. Lu, Y. Yuan. Long-cycling Zinc Metal Anodes Enabled by an In Situ Constructed ZnO Coating Layer, Adv. Funct. Mater., 34 (2024). https://doi.org/10.1002/adfm.202312220.

[78] P. Liang, J. Yi, X. Liu, K. Wu, Z. Wang, J. Cui, Y. Liu, Y. Wang, Y. Xia, J. Zhang. Highly Reversible Zn Anode Enabled by Controllable Formation of Nucleation Sites for Zn-Based Batteries, Adv. Funct. Mater., 30 (2020). https://doi.org/10.1002/adfm.201908528.

[79] S. Sun, Y. Wen, A. Billings, R. Rajabi, B. Wang, K. Zhang, K. Huang. Protecting Zn anodes by atomic layer deposition of ZrO_2 to extend the lifetime of aqueous Zn-ion batteries, Energy Advances, 3 (2024), 299–306. https://doi.org/10.1039/D3YA00400G.

[80] Y. Liu, T. Guo, Q. Liu, F. Xiong, M. Huang, Y. An, J. Wang, Q. An, C. Liu, L. Mai. Ultrathin ZrO_2 coating layer regulates Zn deposition and raises long-life performance of aqueous Zn batteries, Mater. Today Energy, 28 (2022), 101056. https://doi.org/10.1016/j.mtener.2022.101056.

[81] K. Zhao, C. Wang, Y. Yu, M. Yan, Q. Wei, P. He, Y. Dong, Z. Zhang, X. Wang, L. Mai. Ultrathin Surface Coating Enables Stabilized Zinc Metal Anode, Adv. Mater. Interfaces, 5 (2018). https://doi.org/10.1002/admi.201800848.

[82] B. Li, J. Xue, X. Lv, R. Zhang, K. Ma, X. Wu, L. Dai, L. Wang, Z. He. A facile coating strategy for high stability aqueous zinc ion batteries: Porous rutile nano-TiO_2 coating on zinc anode, Surf. Coat. Technol., 421 (2021), 127367. https://doi.org/10.1016/j.surfcoat.2021.127367.

[83] N. Naresh, S. Eom, S. Hwan Jeong, S. Jun Lee, S. Hyeon Park, J. Park, J.-H. Ahn, J.-H. Kim, Y. Hwa Jung. Dendrite-free Zn anodes enabled by a hierarchical zincophilic TiO_2 layer for rechargeable aqueous zinc-ion batteries, Appl. Surf. Sci., 606 (2022), 154932. https://doi.org/10.1016/j.apsusc.2022.154932.

[84] P. Ye, X. Li, K. He, A. Dou, X. Wang, A. Naveed, Y. Zhou, M. Su, P. Zhang, Y. Liu. A semi-interpenetrating network polymer coating for dendrite-free Zn anodes, J. Power Sources, 558 (2023), 232622. https://doi.org/10.1016/j.jpowsour.2022.232622.

[85] X. Cai, W. Tian, Z. Zhang, Y. Sun, L. Yang, H. Mu, C. Lian, H. Qiu. Polymer Coating with Balanced Coordination Strength and Ion Conductivity for Dendrite-Free Zinc Anode, Advanced Materials, 36 (2024). https://doi.org/10.1002/adma.202307727.

[86] P. Chen, X. Yuan, Y. Xia, Y. Zhang, L. Fu, L. Liu, N. Yu, Q. Huang, B. Wang, X. Hu, Y. Wu, T. van Ree. An Artificial Polyacrylonitrile Coating Layer Confining Zinc Dendrite Growth for Highly Reversible Aqueous Zinc-Based Batteries, Advanced Science, 8 (2021). https://doi.org/10.1002/advs.202100309.

[87] Z. Hu, X. Wang, W. Du, Z. Zhang, Y. Tang, M. Ye, Y. Zhang, X. Liu, Z. Wen, C. C. Li. Crowding Effect-Induced Zinc-Enriched/Water-Lean Polymer Interfacial Layer Toward Practical Zn-Iodine Batteries, ACS Nano, 17 (2023), 23207–23219. https://doi.org/10.1021/acsnano.3c10081.

[88] J. Shin, J. K. Seo, R. Yaylian, A. Huang, Y. S. Meng. A review on mechanistic understanding of MnO_2 in aqueous electrolyte for electrical energy storage systems, International Materials Reviews, 65 (2020), 356–387. https://doi.org/10.1080/09506608.2019.1653520.

[89] D. Akinyele, J. Belikov, Y. Levron, Battery Storage Technologies for Electrical Applications: Impact in Stand-Alone Photovoltaic Systems, Energies (Basel), 10 (2017), 1760. https://doi.org/10.3390/en10111760.

[90] J. Song, K. Xu, N. Liu, D. Reed, X. Li. Crossroads in the renaissance of rechargeable aqueous zinc batteries, Materials Today, 45 (2021), 191–212. https://doi.org/10.1016/j.mattod.2020.12.003.

[91] L. Urry. Alkaline deferred action cell, US2970180 (A), 1959.

[92] T. Takamura. PRIMARY BATTERIES – AQUEOUS SYSTEMS | Alkaline Manganese–Zinc, in: Encyclopedia of Electrochemical Power Sources, Elsevier, 2009: pp. 28–42. https://doi.org/10.1016/B978-044452745-5.00098-8.

[93] SAFETY DATA SHEET, (2014).

[94] G. G. Yadav, J. W. Gallaway, D. E. Turney, M. Nyce, J. Huang, X. Wei, S. Banerjee. Regenerable Cu-intercalated MnO2 layered cathode for highly cyclable energy dense batteries, Nat. Commun., 8 (2017), 14424. https://doi.org/10.1038/ncomms14424.

[95] L. Bai, D. Y. Qu, B. E. Conway, Y. H. Zhou, G. Chowdhury, W. A. Adams. Rechargeability of a Chemically Modified MnO_2/Zn Battery System at Practically Favorable Power Levels, J. Electrochem. Soc., 140 (1993), 884–889. https://doi.org/10.1149/1.2056222.

[96] B. B. Owens, P. Reale, B. Scrosati. PRIMARY BATTERIES | Overview, in: Encyclopedia of Electrochemical Power Sources, Elsevier, 2009: pp. 22–27. https://doi.org/10.1016/B978-044452745-5.00096-4.

[97] M. J. D'Ambrose, D. E. Turney, G. G. Yadav, M. Nyce, S. Banerjee. Material Failure Mechanisms of Alkaline Zn Rechargeable Conversion Electrodes, ACS Appl. Energy Mater., 4 (2021), 3381–3392. https://doi.org/10.1021/acsaem.0c03144.

[98] B. J. Hertzberg, A. Huang, A. Hsieh, M. Chamoun, G. Davies, J. K. Seo, Z. Zhong, M. Croft, C. Erdonmez, Y. S. Meng, D. Steingart. Effect of Multiple Cation Electrolyte

Mixtures on Rechargeable Zn–MnO_2 Alkaline Battery, Chemistry of Materials, 28 (2016), 4536–4545. https://doi.org/10.1021/acs.chemmater.6b00232.

[99] A. M. Bruck, M. A. Kim, L. Ma, S. N. Ehrlich, J. S. Okasinski, J. W. Gallaway. Bismuth Enables the Formation of Disordered Birnessite in Rechargeable Alkaline Batteries, J. Electrochem. Soc., 167 (2020), 110514. https://doi.org/10.1149/1945-7111/aba075.

[100] E. D. Rus, G. D. Moon, J. Bai, D. A. Steingart, C. K. Erdonmez. Electrochemical Behavior of Electrolytic Manganese Dioxide in Aqueous KOH and LiOH Solutions: A Comparative Study, J. Electrochem. Soc., 163 (2016), A356–A363. https://doi.org/10.1149/2.1011602jes.

[101] M. Kelly, J. Duay, T.N. Lambert, R. Aidun. Impact of Triethanolamine as an Additive for Rechargeable Alkaline Zn/MnO_2 Batteries under Limited Depth of Discharge Conditions, J. Electrochem. Soc., 164 (2017), A3684–A3691. https://doi.org/10.1149/2.0641714jes.

[102] M. Minakshi, P. Singh. Synergistic effect of additives on electrochemical properties of MnO_2 cathode in aqueous rechargeable batteries, Journal of Solid State Electrochemistry, 16 (2012), 1487–1492. https://doi.org/10.1007/s10008-011-1547-9.

[103] N. D. Ingale, J. W. Gallaway, M. Nyce, A. Couzis, S. Banerjee. Rechargeability and economic aspects of alkaline zinc-manganese dioxide cells for electrical storage and load leveling, J. Power Sources, 276 (2015), 7–18. https://doi.org/10.1016/j.jpowsour.2014.11.010.

[104] A. Poosapati, S. Vadnala, K. Negrete, Y. Lan, J. Hutchison, M. Zupan, D. Madan. Rechargeable Zinc-Electrolytic Manganese Dioxide (EMD) Battery with a Flexible Chitosan-Alkaline Electrolyte, ACS Appl. Energy Mater., 4 (2021), 4248–4258. https://doi.org/10.1021/acsaem.1c00675.

[105] M. Minakshi, D. Ralph. A Novel Sodium-Ion Rechargeable Battery, ECS Trans., 45 (2013), 95–102. https://doi.org/10.1149/04529.0095ecst.

[106] Z. Wei, J. Cheng, R. Wang, Y. Li, Y. Ren. From spent Zn–MnO2 primary batteries to rechargeable Zn–MnO_2 batteries: A novel directly recycling route with high battery performance, J. Environ. Manage., 298 (2021), 113473. https://doi.org/10.1016/j.jenvman.2021.113473.

[107] V. Soundharrajan, B. Sambandam, S. Kim, S. Islam, J. Jo, S. Kim, V. Mathew, Y. Sun, J. Kim. The dominant role of Mn2+ additive on the electrochemical reaction in ZnMn2O4 cathode for aqueous zinc-ion batteries, Energy Storage Mater,. 28 (2020), 407–417. https://doi.org/10.1016/j.ensm.2019.12.021.

[108] C. Wang, Y. Zeng, X. Xiao, S. Wu, G. Zhong, K. Xu, Z. Wei, W. Su, X. Lu. γ-MnO_2 nanorods/graphene composite as efficient cathode for advanced rechargeable aqueous zinc-ion battery, Journal of Energy Chemistry, 43 (2020), 182–187. https://doi.org/10.1016/j.jechem.2019.08.011.

[109] J.-W. Lee, S.-D. Seo, D.-W. Kim. Comparative study on ternary spinel cathode Zn–Mn–O microspheres for aqueous rechargeable zinc-ion batteries, J. Alloys Compd., 800 (2019), 478–482. https://doi.org/10.1016/j.jallcom.2019.06.051.

[110] D. Xu, B. Li, C. Wei, Y.-B. He, H. Du, X. Chu, X. Qin, Q.-H. Yang, F. Kang. Preparation and Characterization of MnO2/acid-treated CNT Nanocomposites for Energy Storage with Zinc Ions, Electrochim. Acta, 133 (2014), 254–261. https://doi.org/10.1016/j.electacta.2014.04.001.

[111] K. Han, F. An, F. Yan, H. Chen, Q. Wan, Y. Liu, P. Li, X. Qu. High-performance aqueous Zn–MnO_2 batteries enabled by the coupling engineering of K^+ pre-intercalation and oxygen defects, J. Mater. Chem. A Mater., 9 (2021), 15637–15647. https://doi.org/10.1039/D1TA03994F.

[112] M. Wang, X. Zheng, X. Zhang, D. Chao, S. Qiao, H. N. Alshareef, Y. Cui, W. Chen. Opportunities of Aqueous Manganese-Based Batteries with Deposition and Stripping Chemistry, Adv. Energy Mater., 11 (2021), 2002904. https://doi.org/10.1002/aenm.202002904.

[113] J. Yang, J. Cao, Y. Peng, W. Yang, S. Barg, Z. Liu, I. A. Kinloch, M. A. Bissett, R. A. W. Dryfe. Unravelling the Mechanism of Rechargeable Aqueous Zn–MnO_2 Batteries: Implementation of Charging Process by Electrodeposition of MnO_2, Chem. Sus. Chem., 13 (2020), 4103–4110. https://doi.org/10.1002/cssc.202001216.

[114] A. Mitha, H. Mi, W. Dong, I. S. Cho, J. Ly, S. Yoo, S. Bang, T. K. A. Hoang, P. Chen. Thixotropic gel electrolyte containing poly(ethylene glycol) with high zinc ion concentration for the secondary aqueous Zn/LiMn2O4 battery, Journal of Electroanalytical Chemistry, 836 (2019), 1–6. https://doi.org/10.1016/j.jelechem.2019.01.014.

[115] C. Qiu, X. Zhu, L. Xue, M. Ni, Y. Zhao, B. Liu, H. Xia. The function of Mn2+ additive in aqueous electrolyte for Zn/δ-MnO_2 battery, Electrochim. Acta, 351 (2020), 136445. https://doi.org/10.1016/j.electacta.2020.136445.

[116] Marcel Pourbaix. Atlas of Electrochemical Equilibria in Aqueous Solutions, 2nd ed., National Association of Corrosion, 1974.

[117] C. Li, X. Xie, S. Liang, J. Zhou. Issues and Future Perspective on Zinc Metal Anode for Rechargeable Aqueous Zinc-ion Batteries, Energy & Environmental Materials, 3 (2020), 146–159. https://doi.org/10.1002/eem2.12067.

[118] M. A. Ibrahim. Improving the throwing power of acidic zinc sulfate electroplating baths, Journal of Chemical Technology & Biotechnology, 75 (2000), 745–755. https://doi.org/10.1002/1097-4660(200008)75:8<745::AID-JCTB274>3.0.CO;2-5.

[119] J. Li. Oxygen Evolution Reaction in Energy Conversion and Storage: Design Strategies Under and Beyond the Energy Scaling Relationship, Nanomicro Lett., 14 (2022), 112. https://doi.org/10.1007/s40820-022-00857-x.

[120] H. Wen, Z. Liu, J. Qiao, R. Chen, G. Qiao, J. Yang. Ultrahigh voltage and energy density aluminum-air battery based on aqueous alkaline-acid hybrid electrolyte, Int. J. Energy Res., 44 (2020), 10652–10661. https://doi.org/10.1002/er.5707.

[121] Y. Wang, W. Pan, S. Luo, X. Zhao, H. Y. H. Kwok, X. Xu, D. Y. C. Leung. High-performance solid-state metal-air batteries with an innovative dual-gel electrolyte, Int. J. Hydrogen Energy, 47 (2022), 15024–15034. https://doi.org/10.1016/j.ijhydene.2022.03.011.

[122] L. Wang, R. Cheng, C. Liu, M. C. Ma, W. Wang, G. Yang, M. K. H. Leung, F. Liu, S. P. Feng. Trielectrolyte aluminum-air cell with high stability and voltage beyond 2.2 V, Materials Today Physics, 14 (2020), 100242. https://doi.org/10.1016/j.mtphys.2020.100242.

[123] B. Chen, D. Y. C. Leung, J. Xuan, H. Wang. A mixed-pH dual-electrolyte microfluidic aluminum-air cell with high performance, Appl. Energy, 185 (2017), 1303–1308. https://doi.org/10.1016/j.apenergy.2015.10.029.

[124] P. Cai, Y. Li, J. Chen, J. Jia, G. Wang, Z. Wen. An Asymmetric-Electrolyte Zn−Air Battery with Ultrahigh Power Density and Energy Density, Chem. Electro. Chem., 5 (2018), 589–592. https://doi.org/10.1002/celc.201701269.

[125] S. Zhao, T. Liu, Y. Dai, Y. Wang, Z. Guo, S. Zhai, J. Yu, C. Zhi, M. Ni. All-in-one and bipolar-membrane-free acid-alkaline hydrogel electrolytes for flexible high-voltage Zn-air batteries, Chemical Engineering Journal, 430 (2022), 132718. https://doi.org/10.1016/j.cej.2021.132718.

[126] K. W. Leong, Y. Wang, W. Pan, S. Luo, X. Zhao, D. Y. C. Leung. Doubling the power output of a Mg-air battery with an acid-salt dual-electrolyte configuration, J. Power Sources, 506 (2021), 230144. https://doi.org/10.1016/j.jpowsour.2021.230144.

[127] Y. Xu, P. Cai, K. Chen, Y. Ding, L. Chen, W. Chen, Z. Wen. High-Voltage Rechargeable Alkali–Acid Zn–PbO_2 Hybrid Battery, Angewandte Chemie International Edition, 59 (2020), 23593–23597. https://doi.org/10.1002/anie.202012017.

[128] T. Gao, Y. Sun, L. Gong, C. Ma, J. Wang, L. Su. 2.8 V Aqueous Lead Dioxide–Zinc Rechargeable Battery Using H_2SO_4 –K_2SO_4 –KOH Three Electrolytes, J. Electrochem. Soc., 167 (2020), 020552. https://doi.org/10.1149/1945-7111/ab6f58.

[129] H. Wu, S.-J. Liu, K. Lian. Aqueous based dual-electrolyte rechargeable Pb–Zn battery with a 2.8 V operating voltage, J. Energy Storage, 29 (2020), 101305. https://doi.org/10.1016/j.est.2020.101305.

[130] F. Yu, L. Pang, X. Wang, E. R. Waclawik, F. Wang, K. (Ken) Ostrikov, H. Wang. Aqueous alkaline–acid hybrid electrolyte for zinc-bromine battery with 3V voltage window, Energy Storage Mater., 19 (2019), 56–61. https://doi.org/10.1016/j.ensm.2019.02.024.

[131] L. Chen, Z. Guo, Y. Xia, Y. Wang. High-voltage aqueous battery approaching 3 V using an acidic-alkaline double electrolyte, Chemical Communications, 49 (2013), 2204. https://doi.org/10.1039/c3cc00064h.

[132] N. Vilas Bôas, J. B. Souza Junior, L. C. Varanda, S. A. S. Machado, M. L. Calegaro. Bismuth and cerium doped cryptomelane-type manganese dioxide nanorods as bifunctional catalysts for rechargeable alkaline metal-air batteries, Appl. Catal. B, 258 (2019), 118014. https://doi.org/10.1016/j.apcatb.2019.118014.

[133] X. Zhang, W. Yang, J. Yang, D. G. Evans. Synthesis and characterization of α-MnO_2 nanowires: Self-assembly and phase transformation to β-MnO_2 microcrystals, J. Cryst. Growth, 310 (2008), 716–722. https://doi.org/10.1016/j.jcrysgro.2007.11.113.

[134] X. Zhang, P. Yu, D. Wang, Y. Ma. Controllable Synthesis of α-MnO_2 Nanostructures and Phase Transformation to β-MnO_2 Microcrystals by Hydrothermal Crystallization, J. Nanosci. Nanotechnol., 10 (2010) 898–904. https://doi.org/10.1166/jnn.2010.1893.

[135] Y. Khan, S. K. Durrani, M. Mehmood, M. R. Khan. Mild hydrothermal synthesis of γ-MnO_2 nanostructures and their phase transformation to α-MnO_2 nanowires, J. Mater. Res., 26 (2011), 2268–2275. https://doi.org/10.1557/jmr.2011.138.

[136] K. Li, C. Chen, H. Zhang, X. Hu, T. Sun, J. Jia. Effects of phase structure of MnO2 and morphology of δ-MnO2 on toluene catalytic oxidation, Appl. Surf. Sci., 496 (2019), 143662. https://doi.org/10.1016/j.apsusc.2019.143662.

[137] H. Song, H. Zhao, X. Zhang, Y. Xu, X. Cheng, S. Gao, L. Huo. A hollow urchin-like α-MnO_2 as an electrochemical sensor for hydrogen peroxide and dopamine with high selectivity and sensitivity, Microchimica Acta, 186 (2019), 210. https://doi.org/10.1007/s00604-019-3316-x.

[138] M. Wang, K. Chen, J. Liu, Q. He, G. Li, F. Li. Efficiently Enhancing Electrocatalytic Activity of α-MnO_2 Nanorods/N-Doped Ketjenblack Carbon for Oxygen Reduction Reaction and Oxygen Evolution Reaction Using Facile Regulated Hydrothermal Treatment, Catalysts, 8 (2018), 138. https://doi.org/10.3390/catal8040138.

[139] Z. Huang, W. Zhou, C. Ouyang, J. Wu, F. Zhang, J. Huang, Y. Gao, J. Chu. High performance of Mn-Co-Ni-O spinel nanofilms sputtered from acetate precursors, Sci. Rep., 5 (2015), 10899. https://doi.org/10.1038/srep10899.

[140] Z. Morgan Chan, D. A. Kitchaev, J. Nelson Weker, C. Schnedermann, K. Lim, G. Ceder, W. Tumas, M. F. Toney, D. G. Nocera. Electrochemical trapping of metastable Mn^{3+} ions for activation of MnO_2 oxygen evolution catalysts, Proceedings of the National Academy of Sciences, 115 (2018). https://doi.org/10.1073/pnas.1722235115.

[141] H. Idriss, On the wrong assignment of the XPS O1s signal at 531–532 eV attributed to oxygen vacancies in photo- and electro-catalysts for water splitting and other materials applications, Surf. Sci., 712 (2021), 121894. https://doi.org/10.1016/j.susc.2021.121894.

[142] L. Jia, F. Li, C. Yang, X. Yang, B. Kou, Y. Xing, J. Peng, G. Ni, Z. Cao, S. Zhang, T. Zhao, X. Jin. Direct Z-Scheme Heterojunction α-MnO2/BiOI with Oxygen-Rich Vacancies Enhanced Photoelectrocatalytic Degradation of Organic Pollutants under Visible Light, Catalysts, 12 (2022), 1596. https://doi.org/10.3390/catal12121596.

[143] T. Hishida, K. Ohbayashi, M. Kobata, E. Ikenaga, T. Sugiyama, K. Kobayashi, M. Okawa, T. Saitoh. Empirical relationship between x-ray photoemission spectra and electrical conductivity in a colossal magnetoresistive manganite La1−*x* Sr *x* MnO3, J. Appl. Phys., 113 (2013). https://doi.org/10.1063/1.4811372.

[144] P. Umek, R. C. Korošec, A. Gloter, U. Pirnat. The control of the diameter and length of α-MnO_2 nanorods by regulation of reaction parameters and their thermogravimetric properties, Mater. Res. Bull., 46 (2011), 278–284. https://doi.org/10.1016/j.materresbull.2010.10.012.

[145] Z. Zheng, G. Yang, J. Yao, J. Li, J. Zheng, Z. Wu, Y. Gan, C. Wang, L. Lv, H. Wan, C. Chen, H. Wang, L. Tao, J. Zhang, H. Wang. High-valence molybdenum promoted proton

migration and inhibited dissolution for long-life aqueous Zn-MnO_2 batteries, Appl. Surf. Sci., 592 (2022), 153335. https://doi.org/10.1016/j.apsusc.2022.153335.

[146] M. Zhou, S. Guo, J. Li, X. Luo, Z. Liu, T. Zhang, X. Cao, M. Long, B. Lu, A. Pan, G. Fang, J. Zhou, S. Liang. Surface-Preferred Crystal Plane for a Stable and Reversible Zinc Anode, Advanced Materials, 33 (2021). https://doi.org/10.1002/adma.202100187.

[147] Y. Song, S. Zhang, C. Zhang, Y. Yang, K. Lv. Raman Spectra and Microstructure of Zinc Oxide irradiated with Swift Heavy Ion, Crystals (Basel), 9 (2019), 395. https://doi.org/10.3390/cryst9080395.

[148] F. Friedrich, N. H. Nickel. Resonant Raman scattering in hydrogen and nitrogen doped ZnO, Appl. Phys. Lett., 91 (2007). https://doi.org/10.1063/1.2783222.

[149] C. Mele, B. Bozzini, Spectroelectrochemical investigation of the anodic and cathodic behaviour of zinc in 5.3 M KOH, J. Appl. Electrochem., 45 (2015), 43–50. https://doi.org/10.1007/s10800-014-0755-2.

[150] S. Hosseini, A. Abbasi, L.-O. Uginet, N. Haustraete, S. Praserthdam, T. Yonezawa, S. Kheawhom. The Influence of Dimethyl Sulfoxide as Electrolyte Additive on Anodic Dissolution of Alkaline Zinc-Air Flow Battery, Sci. Rep., 9 (2019), 14958. https://doi.org/10.1038/s41598-019-51412-5.

[151] P. He, J. Huang. Detrimental Effects of Surface Imperfections and Unpolished Edges on the Cycling Stability of a Zinc Foil Anode, ACS Energy Lett., 6 (2021), 1990–1995. https://doi.org/10.1021/acsenergylett.1c00638.

[152] C. Hitz, A. Lasia. Experimental study and modeling of impedance of the her on porous Ni electrodes, Journal of Electroanalytical Chemistry, 500 (2001), 213–222. https://doi.org/10.1016/S0022-0728(00)00317-X.

[153] L. Birry, A. Lasia. Studies of the Hydrogen Evolution Reaction on Raney Nickel–Molybdenum Electrodes, J. Appl. Electrochem., 34 (2004), 735–749. https://doi.org/10.1023/B:JACH.0000031161.26544.6a.

[154] C. F. Bischoff, O. S. Fitz, J. Burns, M. Bauer, H. Gentischer, K. P. Birke, H.-M. Henning, D. Biro. Revealing the Local pH Value Changes of Acidic Aqueous Zinc Ion Batteries with a Manganese Dioxide Electrode during Cycling, J. Electrochem. Soc., 167 (2020), 020545. https://doi.org/10.1149/1945-7111/ab6c57.

Ramona Zukule (née Dūrena) was born on 18 December 1996 in Limbaži. She obtained a Bachelor's degree in Chemical Technology (2019) and a Master's degree in Nanomaterials Technologies (2021) from Riga Technical University (RTU). Since 2021, she has been pursuing doctoral studies at RTU, focusing on water-based zinc–manganese dioxide ($Zn\text{-}MnO_2$) batteries, their electrolyte modifications, and electrode stabilization mechanisms. From 2022 to 2024, she was a researcher at RTU and participated in the FLPP project "Investigation of electrodes and electrolytes for obtaining amphoteric decoupled rechargeable batteries." She has also worked at the Institute of Solid State Physics, University of Latvia, and since February 2025, has been a patent attorney assistant at AAA Law Latvia Ltd. Her scientific interests are related to the development of water-based $Zn\text{-}MnO_2$ batteries, the study of electrode-electrolyte interactions, and the application of nanomaterials in electrochemical systems.